May 2015

Validation, Calibration, and Improvement of Remote Sensing ET Algorithms in Mountainous Regions Using Scintillometers

WRRI Technical Completion Report No. 366

Jan M.H. Hendrickx
Jan Kleissl

The scintillometer research team, from left: Kim Bandy, Jan Hendrickx, Whitney Defoor, Jesus Gomez, and Jan Kleissl. Field photo by George Zamora, NM Tech.

NEW MEXICO WATER RESOURCES RESEARCH INSTITUTE
New Mexico State University
MSC 3167, PO Box 30001
Las Cruces, New Mexico 88003-0001
(575) 646-4337 email: nmwrri@wrri.nmsu.edu

VALIDATION, CALIBRATION, AND IMPROVEMENT OF REMOTE SENSING ET ALGORITHMS IN MOUNTAINOUS REGIONS USING SCINTILLOMETERS

By

Jan M.H. Hendrickx
Hydrology Program
Department of Earth & Environmental Science
New Mexico Tech

Jan Kleissl
Department of Mechanical and Aerospace Engineering
University of California at San Diego
(Formerly at Hydrology Program
Department of Earth & Environmental Science
New Mexico Tech)

TECHNICAL COMPLETION REPORT

Project No. 111054

May 2015

New Mexico Water Resources Research Institute.

The research on which this report is based was financed in part by the U.S. Department of the Interior, Geological Survey (award 06HQGR0187), through the New Mexico Water Resources Research Institute (contract Q01112). Other sponsors also have contributed to this study: NSF EPSCoR grant EPS-0447691; U.S. Department of Agriculture, CSREES grant No.: 2003-35102-13654; and the NSF Science and Technology Center program Sustainability of Semi-Arid Hydrology and Riparian Areas (SAHRA; EAR-4619876800).

DISCLAIMER

The purpose of the Water Resources Research Institute technical reports is to provide a timely outlet for research results obtained on projects supported in whole or in part by the institute. Through these reports, we are promoting the free exchange of information and ideas, and hope to stimulate thoughtful discussions and actions that may lead to resolution of water problems. The WRRI, through peer review of draft reports, attempts to substantiate the accuracy of information contained within its reports, but the views expressed are those of the authors and do not necessarily reflect those of the WRRI or reviewers. Contents of this publication do not necessarily reflect the views and policies of the Department of the Interior, nor does the mention of trade names or commercial products constitute their endorsement by the United States government.

ACKNOWLEDGEMENTS

This research was supported by USGS award 06HQGR0187 and NMSU-WRRI contract Q01112. Other sponsors also have contributed to this study by financing some of the seven scintillometers deployed in this study: NSF EPSCoR grant EPS-0447691; U.S. Department of Agriculture, CSREES grant No.: 2003-35102-13654; and the NSF Science and Technology Center program Sustainability of Semi-Arid Hydrology and Riparian Areas (SAHRA; EAR-4619876800).

We are indebted to the Sevilleta National Wildlife Refuge staff and affiliated scientists, in particular Renee Robichaud, Don Natvig, Renee Brown, and Mike Friggens for assistance with preparation and execution of the experiments.

Without Bob Parmenter and his staff at the Valles Caldera National Preserve, our experiments would not have been possible. Assistance in the field by Kathy Fleming, Kimberly Bandy, and Jack Cheney is acknowledged.

ABSTRACT

The overall goal of this study was to improve the remote sensing estimates of evapotranspiration in mountainous regions by field studies at New Mexico sites that are representative of large parts of the mountainous regions in the arid southwest. In particular, we proposed to validate sensible and latent heat fluxes estimated from the remote sensing Surface Energy Balance Algorithms for Land (SEBAL) model using large aperture scintillometer (LAS) ground measurements over mountainous landscapes in New Mexico. Unfortunately, research is not always predictable. In our study, shortly after the award of the grant we suspected and later confirmed with inter-comparison measurements that the sensible heat flux measurements by the ten large aperture Kipp & Zonen scintillometers of Hendrickx's research group contained a considerable inter-instrument error. Therefore, we had no choice but to shift the focus of the study toward (1) conducting a rigorous quantitative inter-comparison study for Kipp & Zonen large aperture scintillometers and (2) testing whether the biased scintillometers can still be used for field energy balance studies. Our conclusions are: (1) the first generation Kipp & Zonen LASs does indeed have a large inter-instrument bias that can exceed 21%; (2) these LASs can be used for field energy balance studies after calibration against a reference LAS or eddy covariance sensible heat flux measurements over homogeneous terrain. Our inter-comparison study by *Kleissl et al.* [2008] has been cited 56 times by studies reconfirming our findings or investigating error causes and remediation. More importantly the manufacturer Kipp & Zonen has redesigned its LAS and has started the production of the next generation LAS without inter-instrument biases. The New Mexico Scintillometer Network has taught us many valuable lessons on how to utilize scintillometry [*Kleissl et al.*, 2009a] for statewide validation of evapotranspiration remote sensing algorithms in New Mexico.

Key words: scintillometer network, sensible heat flux, SEBAL, METRIC, New Mexico

TABLE OF CONTENTS

DISCLAIMER	ii
ACKNOWLEDGEMENTS	iii
ABSTRACT	iv
TABLE OF CONTENTS	v
LIST OF TABLES	vi
LIST OF FIGURES	vi
LIST OF ABBREVIATIONS AND ACRONYMS	viii
1. INTRODUCTION	1
2. SCINTILLOMETRY	4
2.1 Instrumentation and Theory	4
2.2 Comparison of Eddy Covariance and Scintillometry	7
2.3 Scintillometer Network in New Mexico	9
3. REMOTE SENSING ALGORITHMS FOR EVAPOTRANSPIRATION	13
3.1 Landsat and MODIS Satellite Imagery	13
3.2 SEBAL/METRIC Algorithms for Evapotranspiration Mapping	16
4. SCINTILLOMETER INTERCOMPARISON EXPERIMENT	20
5. LESSONS LEARNED	29
REFERENCES	31

LIST OF TABLES

Table 1.	New Mexico Tech large aperture scintillometer (LAS) network [Kleissl et al., 2009a]. Coordinates of the locations are given in UTM 13 WGS84.	11
Table 2.	Band spatial resolutions (m) and wavelengths (μm) of Landsat 7 and MODIS sensors.	14
Table 3.	Experimental setup and LAS instruments used for intercomparison over nearly horizontal beams in the Valles Caldera National Park (after *Kleissl et al.* [2008]). The effective beam height is calculated for free convective conditions and the distance is measured between the receiver and the transmitter.	22
Table 4.	Linear regression slopes and 95% confidence intervals of sensible heat fluxes between LAS-LAS and LAS-EC for the experiments H1 and H2 in unstable conditions [*Kleissl et al.*, 2008].	26

LIST OF FIGURES

Figure 1.	Validation of SEBAL in the Rio Grande (NM), San Pedro (AZ), and Owens riparian river valleys (Hendrickx and Hong, 2005). Each point compares the ET (mm/day) from SEBAL against the ET (mm/day) measured with eddy covariance.	3
Figure 2.	An ET map of the South Valley of Albuquerque for a 22x32 km riparian, irrigated, desert, and urban area from LandSat7 (at 30 m resolution) and MODIS (at 1000 m resolution). Note the good agreement between the two ET maps.	3
Figure 3.	Two LASs (one receiver and one transmitter) during the Scintillometer Intercomparison study in northern NM. The corresponding transmitter and receiver are 2 km away.	5
Figure 4.	Layout of scintillometer system and illustration of turbulent structures that cause beam refraction on density variations [*Kleissl et al.*, 2009a].	5
Figure 5.	Typical footprint weighting function (color) for a LAS transect (white line) at the El Malpais National Monument, NM. The transect length is 2.9 km and its height above the land surface is 60 m. Note the differences in vertical scales. The footprint under perpendicular wind direction is larger than under parallel wind direction [*Meijninger et al.*, 2002].	10
Figure 6.	Examples of LAS setup locations in New Mexico in moist riparian areas and mountainous grasslands and dry deserts and lava flows.	10
Figure 7.	Locations of LAS transects in the New Mexico scintillometer network in March 2007.	12
Figure 8.	Intercomparison of sensible heat flux measurements from three LASs (symbols), EC (purple line), and net radiation (black line) in December 2005. The LAS measurements agree well with EC and provide a much smoother time series.	12

Figure 9.	Landsat and MODIS satellite imagery covering the Middle Rio Grande valley on June 16, 2002.	15
Figure 10.	Photograph of experimental site at the Valles Calder33a National Preserve: northwest end of the transects of experiment H1 looking southeast. The instruments at the other end of the transect are invisible in a clearing on the opposite site of the valley [*Kleissl et al.*, 2008].	22
Figure 11.	Profile of the transects used in experiments H1 and H2. The legend gives the last two digits of the LAS serial number (Table 3). Receivers and transmitters were alternated at each site [*Kleissl et al.*, 2008].	23
Figure 12.	Example time series of the net radiation (R_{net} rescaled by 1/2) and sensible heat flux H from LAS and EC for experiment H1 on June 19, 2006 [*Kleissl et al.*, 2008].	24
Figure 13.	Scatter plots of sensible heat flux measurements from serial number $^{0300}05$ (x-axis) vs the other LASs (only the last two digits of the serial number are shown in the axis labels) for experiment H1. The text indicates the linear fit, mean absolute deviation (MAD in Wm^{-2}), correlation coefficient ρ, and number of samples N. The grey dashed line is the 1:1 line [*Kleissl et al.*, 2008].	25
Figure 14.	(top) Time series of LAS-measured sensible heat fluxes H and (bottom) global solar radiation on 17 Sep 2006. SEBAL estimates at the MODIS overpass time (1035 LST) are presented with crosses for each site. (a) On this sunny day in New Mexico, peaks of H range from less than 100 W m^{-2} over an irrigated alfalfa field (SAA) to 400 W m^{-2} over low-albedo lava flows (EMNM). Note that the EMRTC cross is right on the purple line and that the Sevilleta (SNWR, red), San Acacia riparian (SAR, green), and SAA (blue) are on top of each other. (b) The solar radiation data show a cloud-free day. SEBAL solar radiation is calculated perpendicular to the local surface, whereas the measurements show global horizontal radiation [*Kleissl et al.*, 2009a]. See Figure 7 for locations of the LAS sites in New Mexico.	28
Figure 15.	Second generation Kipp & Zonen LAS of New Mexico Tech during calibration in The Netherlands in April 2015.	28

LIST OF ABBREVIATIONS AND ACRONYMS

ALEXI	Atmosphere-Land Exchange Inverse model
C_n^2	Structure parameter of air refractive index
CSAT3	Campbell Scientific 3D sonic anemometer
C_T^2	Structure parameter of air temperature
DGPS	Differential Global Positioning System
EC	Eddy Covariancy system to measure sensible and latent heat fluxes
EF	Evaporative Fraction
ET	Evapotranspiration
ETrF	Reference ET Fraction
GPS-WAAS	Global Positioning System Wide Area Augmentation System
IRGA	Infrared Gas Analyzer
LAS	Large Aperture Scintillometer
LIS	Land Information System
METRIC	Mapping ET at high spatial Resolution with Internalized Calibration model
MODIS	Moderate Resolution Imaging Spectroradiometer
MOD16	MODIS global evapotranspiration product
NDVI	Normalized Difference Vegetation Index
NLDAS	North American Land Data Assimilation Systems
NMWRRI	New Mexico Water Resources Research Institute
SAVI	Soil Adjusted Vegetation Index
SEBAL	Surface Energy Balance Algorithms for Land as implemented in New Mexico model
USGS	U.S. Geological Survey

1. INTRODUCTION

Accounting of key reservoirs and fluxes associated with the global water and energy cycle, including their spatial and temporal variability, are crucial goals of the U.S. Geological Survey and water resources managers. High accuracy in these flux estimates is of particular importance for water management in semi-arid regions with frequent water scarcity.

During the last two decades, many investigators have explored the application of satellite optical (i.e., visible, near- and mid-infrared, thermal infrared) remote sensing for the estimation of regional evapotranspiration (ET) distributions [*Choudhury*, 1989; *Kustas and Norman*, 1996; *Moran and Jackson*, 1991]. These efforts have resulted in the development of several operational remote sensing ET algorithms that are now being used by researchers and practitioners on a routine basis. Examples are: SEBAL (Surface Energy Balance Algorithms for Land as implemented in New Mexico) [*Bastiaanssen et al.*, 1998a; *Bastiaanssen et al.*, 2005; *Bastiaanssen et al.*, 1998b], METRIC (Mapping ET at high spatial Resolution with Internalized Calibration) [*Allen et al.*, 2007a; *Allen et al.*, 2007b; *Allen et al.*, 2011; *Allen et al.*, 2008b], ALEXI (Atmosphere-Land Exchange Inverse) [*Anderson et al.*, 1997], NLDAS (North American Land Data Assimilation Systems), LIS (Land Information Systems) [*Kumar et al.*, 2008; *Peters Lidard et al.*, 2004] and the MODIS global evapotranspiration product MOD16 [*Mu et al.*, 2011; *Mu et al.*, 2007] . Although these algorithms are quite different in their spatial and temporal scales (30 m to 1/8th degree or about 13 km in New Mexico, daily to monthly), they all have produced ET maps on local, regional, or national scales that are being used by hydrologists and water resources professionals.

However, these remote sensing algorithms have encountered significant difficulties in accurately estimating evapotranspiration (ET) in mountainous regions that are characterized by heterogeneous soil and topography, and high elevation changes [*Allen and Anderson*, January 2005]. Mountains cover approximately 25% of the world's land area, accommodate 26% of global population, and generate 32% of surface runoff [*Meybeck et al.*, 2001]. However, mountain runoff represents more than 90% of the total runoff in the semi-arid basins of the Rio Grande, Oranje, Colorado, and Rio Negro rivers. The often heavy precipitation in the mountains drives river runoff and downstream groundwater recharge, both important water supplies for irrigation.

Mountains also act as a buffer in the water supply system, as precipitation often occurs as snow and can be stored for several months and gradually released. In the western U.S. over 60 million people depend on mountain river basins for their water supplies and generally in semi-arid mountainous regions the greatest flux of water out of the system is ET [*Bales et al.*, 2004].

The availability of ET maps for mountain areas will fill many societal needs: (1) standardized input to water balances of weather, flood, and fire hazard forecasting models and input to general circulation models, including model initialization, which will lead to improved prediction of available moisture, rainfall, and fire hazards; (2) mapping of water deficits and reductions in agricultural and forest production caused by drought; (3) estimates of mountain recharge to groundwater systems; (4) inputs to state and federal water resources management and planning models to improve resource and endangered species management and increase program operational efficiencies; and (5) standardized input to hydrologic research models. Therefore, the overall goal of this study is to improve the remote sensing estimates of ET in mountainous regions by field studies at New Mexico sites that are representative for large parts of the mountainous regions in the arid southwest.

Hendrickx's research team uses the SEBAL and METRIC algorithms to process remote sensing data to compute ET using the surface energy balance [*Allen et al.*, 2011] (Figs. 1-2). When applied to Landsat images these algorithms produce maps of ET with a resolution of 30m. SEBAL and METRIC have been accepted in the western United States because of the use of internalized calibration procedures [*Allen et al.*, 2010; *Allen et al.*, 2007b; *Allen et al.*, 2008a; *Bastiaanssen et al.*, 2005]. These procedures index sensible heat flux from the land surface (one of the major energy balance components) to satellite measured surface temperatures at specific surface boundary conditions. The indexing of the heat flux eliminates to a large extent the need for atmospheric correction of short-wave and thermal information in images [*Tasumi et al.*, 2003].

Issues that are not well defined for mountainous regions in our current applications of SEBAL and METRIC for evaluation of sensible and latent heat fluxes are: (1) how to scale surface temperatures measured at different elevations back to one reference surface temperature in SEBAL; and (2) what wind speeds and surface roughnesses should be assigned to mountain pixels. To address these issues, we proposed in 2006 to measure the sensible heat flux over several transects on mountains slopes, ridges, and highlands using the novel measurement technique of scintillometry

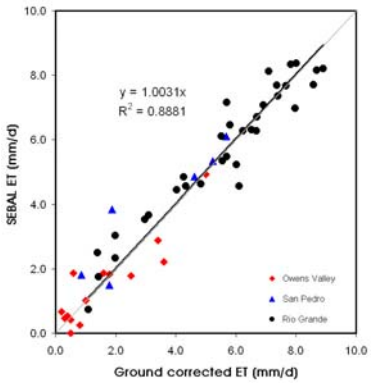

Figure 1. Validation of SEBAL in the Rio Grande (NM), San Pedro (AZ), and Owens riparian river valleys (Hendrickx and Hong, 2005). Each point compares the ET (mm/day) from SEBAL against the ET (mm/day) measured with eddy covariance.

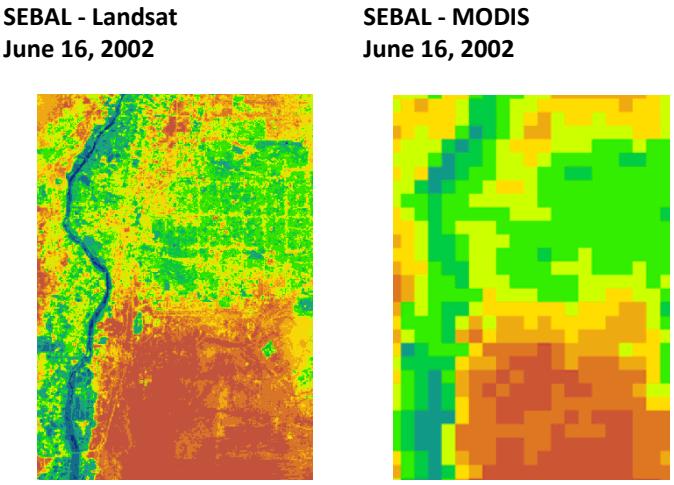

Figure 2. An ET map of the South Valley of Albuquerque for a 22x32 km riparian, irrigated, desert, and urban area from LandSat7 (at 30 m resolution) and MODIS (at 1000 m resolution). Note the good agreement between the two ET maps.

[*De Bruin*, 2002; *Hartogensis*, 2006; *Hemakumara et al.*, 2003; *Hendrickx et al.*, 2007; *Meijninger*, 2003; *Meijninger and Bruin*, 2000; *Meijninger et al.*, 2002; *Moene et al.*, 2004; *Tasumi et al.*, 2003]. In particular, we proposed to pursue the following objectives: (1) validate sensible and latent heat fluxes estimated from SEBAL using scintillometer ground measurements over mountainous landscapes in New Mexico; (2) calibrate SEBAL satellite ET maps using sensible heat flux measurements over scintillometer transects in near real time; and (3) develop improvements for SEBAL and other remote sensing ET algorithms for better ET estimates in mountainous areas.

Unfortunately, research is not always predictable. In our study, shortly after the award of the USGS/NMWRRI grant, we suspected and later confirmed with intercomparison measurements that the sensible heat flux measurements by the ten large aperture Kipp & Zonen scintillometers of Hendrickx's research group contain a considerable inter-instrument error that can exceed 20%. Therefore, we had no choice but to shift the focus of the study toward testing whether the biased scintillometers can still be used for field energy balance studies and the improvement of remote sensing ET algorithms for mountainous areas without using scintillometry. The next two sections of this final report explain the promising new technology of scintillometry for measurements of the

sensible heat flux on the pixel scale (500 to 5000 m) as well as the SEBAL/METRIC approach for regional mapping of evapotranspiration using Landsat and MODIS images. Then, we discuss our intercomparison study and how it led to an improved design of the next generation of Kipp & Zonen scintillometers. The final section presents "lessons learned" for the use of scintillometers for calibration of remote sensing ET algorithm in New Mexico and the conclusions of our investigations.

2. SCINTILLOMETRY

2.1 Instrumentation and Theory

A large aperture scintillometer (LAS) is an instrument that consists of a laser transmitter and a receiver (Figs. 3 and 4). The receiver measures intensity fluctuations in the radiation emitted by the transmitter caused by refractive scattering by turbulent eddies in the LAS path. For LASs, the observed intensity fluctuations are a measure of the structure parameter of the refractive index, C_n^2. At optical wavelengths the contribution of temperature fluctuations dominates, that is, the structure parameter of temperature C_T^2 can be deduced from C_n^2. For radio wavelengths (> 1 mm) on the other hand, water vapor fluctuations contribute most to the scintillometer signal fluctuation, that is, the structure parameter of water vapor C_q^2 can be deduced from C_n^2. Using similarity theory in the atmospheric surface layer, surface fluxes of sensible heat H, latent heat λET and momentum can be determined from C_T^2 and C_q^2 and supplemental meteorological measurements.

Different scintillometers have been developed for the measurement of surface fluxes of momentum, sensible heat, and water vapor using different wavelengths, aperture sizes and configurations [*Andreas*, 1989; 1990; *Hill*, 1992; *Hill et al.*, 1992a; b; *Khosiek and Herben*, 1983; *Thiermann and Grassl*, 1992; *Wesely*, 1976a]. In this study we used the LAS with an aperture size D of 15 cm, wavelength of laser beam 880 nm, and pathlength L between 0.5 – 5.0 km. For this scintillometer, C_n^2 is dominated by the structure parameter of temperature C_t^2. The scintillometer measures the beam-average of C_n^2 between emitter and receiver weighted by a spatial bell-shaped function. $\overline{C_n^2}$ is related to the variance of the logarithm of the intensity fluctuations of the measured light intensity $\sigma^2_{ln(i)}$ as follows ([*Wang et al.*, 1978]

Figure 3. Two LASs (one receiver and one transmitter) during the Scintillometer Intercomparison study in northern NM. The corresponding transmitter and receiver are 2 km away.

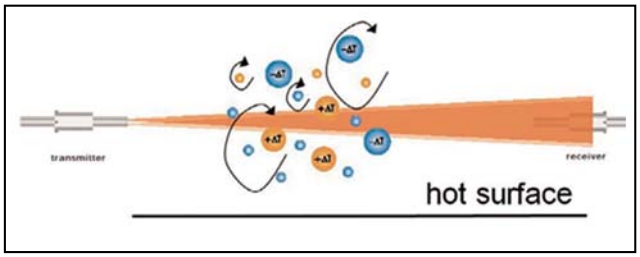

Figure 4. Layout of scintillometer system and illustration of turbulent structures that cause beam refraction on density variations [*Kleissl et al.*, 2009a].

$$\overline{C_n^2} = 1.12\,\sigma_{\ln(I)}^2\; D^{7/3}\; L^{-3} \qquad (1)$$

For a LAS operating at 880 nm the C_n^2 is related to C_T^2 as [*Wesely*, 1976a; *Wesely*, 1976b]

$$C_T^2 = C_n^2 \left(\frac{T^2}{-0.78\times10^{-6}\; P} \right)^2 \left(1 + \frac{0.03}{\beta} \right)^{-2} \qquad (2)$$

where T is the absolute air temperature, P is the atmospheric pressure, and β the Bowen-ratio. Once C_T^2 is obtained, the sensible heat flux is obtained iteratively from the following equations assuming atmospheric surface layer similarity theory

$$\frac{C_T^2 (z_{LAS} - d)^{2/3}}{T_*^2} = f_T\left(\frac{z_{LAS} - d}{L_{MO}} \right) = f_T(\zeta) \qquad (3)$$

$$T_* = -\frac{H}{\rho\, c_p\, u_*} \tag{4}$$

$$L_{MO} = \frac{u_*\, T}{g\, \kappa\, T_*} \tag{5}$$

$f_T = 4.9 * (1 - 6.1\, \zeta)^{-2/3}$ and $f_T = 4.9 * (1 + 2.2\, \zeta^{2/3})$ are the universal stability correction functions for unstable and stable conditions. z_{LAS} is the height of the laser beam above the soil surface, $\kappa = 0.4$ is the von Karman constant, g is acceleration of gravity, c_p is the specific heat at constant pressure, ρ is the density of air, and L_{MO} is the Obukhov length. The friction velocity u_* is derived from estimates of the roughness length z_o, zero displacement height d, and stability correction functions [*Panofsky and Dutton*, 1984].

At first sight, there seems to be a large number of parameters required to derive H from C_T^2, which if they needed to be determined over the LAS transect would require a lot of additional measurements and introduce uncertainty. However, it turns out [*Hartogensis et al.*, 2003] that their influence on the resulting sensible heat flux is small (10% or less) and a single measurement of wind speed, temperature, and atmospheric pressure is sufficient. The latter parameter can often more easily be obtained from nearby weather stations or from mesoscale atmospheric models. For free convective conditions often encountered in the southwestern USA, u* (and thus wind speed and roughness length) are no longer needed to calculate H.

Since similarity theory is used in the derivation of the sensible heat flux, surface homogeneity over the footprint area is required in principle, since no significant horizontal flux transport term or storage flux should exist. However, it has been demonstrated that a LAS sensible heat flux over a chessboard pattern of crop matched the weighted average of the individual crop sensible heat fluxes measured by the eddy covariance method (EC) [*Beyrich et al.*, 2002; *Meijninger et al.*, 2002]. These studies showed that the LAS should be located above the blending height of individual heterogeneities for similarity theory to hold.

For a full description of the theory behind scintillometry, we refer to the October issue of Boundary-Layer Meteorology (2002; vol. 105-1) by guest editor Dr. Henk de Bruin on Recent Developments in Scintillometry Research. In spite of the complex physics on which scintillometers

are based, their operation and data analysis are relatively simple compared to that of eddy covariance systems. Therefore, LAS systems have the potential to become a standard hydrologic instrument just as a rain gauge or thermometer. Their main advantage over eddy covariance and Bowen ratio measurements is that they provide real-time measurements with five minutes temporal resolution at the spatial scale of the pixel or a set of pixels in a satellite image. Our study builds on experiences gained in the White Volta Basin where sensible heat fluxes have been measured along transects of several kilometers using scintillometers [*Hafeez et al.*, 2006; *Marx*, 2003; *Schüttemeyer et al.*, 2006]. The results of these studies indicate that the use of scintillometer measurements over dry and moist pixels holds much potential to increase the reliability of parameterizations for remote sensing energy balance algorithms.

2.2 Comparison of Eddy Covariance and Scintillometry

A major difficulty for the further development and validation of hydrologic and meteorological remote sensing algorithms has been the scale gap between existing surface flux measurement footprints using the eddy covariance method (EC) and the pixel size of readily available imagery from Landsat (30-60 m) and MODIS (250-1000 m). Scintillometers make it possible to measure sensible and latent heat fluxes over distances of 100 to 10,000 m and, thus, to bridge the scale gap.

EC is often the technique of choice for turbulent surface heat flux measurements in the atmospheric surface layer [*Evett*, 2000]. An EC system typically consists of a 3D sonic anemometer operated at >= 10 hz and a scalar sensor in close proximity. The sensible heat flux is then measured directly from covariances in the vertical velocity w and temperature T as $H=\rho c_p\langle w'T'\rangle$ where w' and T' are, respectively, the difference between the mean wind velocity and air temperature during an averaging period commensurate with the low frequency eddies, typically between 15 to 60 minutes and the instantaneous measurements at frequency of >= 10 Hz. However, several corrections have to be applied to the measurements and even then turbulent fluxes from EC systems are typically smaller than the available energy, that is, the difference between net radiation and soil heat flux. This issue is known as energy balance closure, which has yet to be resolved [*Allen*, 1999; *Foken et al.*, 2006a; b; *Twine et al.*, 2000].

EC flux measurement uncertainties have been examined in detail by comparing laboratory and field data of sonic anemometer-thermometers (SAT) from eight different manufacturers

[*Loescher et al.*, 2005]. Based on an idealized setup of SATs and great care going into data collection and processing, they found that uncertainty in <w'T'> among SATs for each 15-min averaging period ranged from -23.1 to +16.1%, and was reduced to -1 to +8% when averaged over 940 15-min periods and corrected for mean temperature offsets. Linear regressions of <w'T'> for seven instruments versus the eighth in neutral, slightly unstable, and unstable stability conditions revealed slopes ranging from 19-31%, while standard deviations of the slopes (i.e., a measure of the expected slope for any two sensors) were between 7-11%. One should note that these uncertainties only apply to cases where great care has been taken in installation and maintenance of the equipment, data processing, and site selection. Larger errors may be expected for non-ideal conditions. Another issue with EC is the variability of the footprint. The 'heat source' area or footprint of EC measurements is highly variable, depending mostly on wind direction and atmospheric stability [*Evett*, 2000; *Horst and Weil*, 1992; *Hsieh et al.*, 2000; *Schmid*, 1994; *Schmid and Oke*, 1990; *Schuepp et al.*, 1990]. Over natural surfaces, which always display some degree of heterogeneity, this together with the uncertainties described above leads to noisy time series of EC turbulent heat fluxes, even for long (30-minute) averaging intervals.

Despite these shortcomings EC systems have represented a significant step ahead compared to previous techniques, allowing examination of atmospheric surface layer turbulence with unprecedented accuracy and robustness, especially over homogeneous surfaces such as agricultural fields. Large global and national funding for field measurements such as Ameriflux have also enabled studies of turbulent land-atmosphere exchange over a variety of ecosystems, which has improved quantification of important processes like CO_2 uptake by boreal forests and evapotranspiration.

The most significant drawback for EC systems, however, is in the context of hydrologic and meteorological modeling. EC systems are typically installed just above the roughness sub-layer for reasons of cost, accessibility, and to limit the footprint area to a homogeneous area. While this assures the representativeness of the measured fluxes to the immediate environment of the tower (where also the non-turbulent flux components of the energy balance, i.e., radiation and soil heat flux, are measured), this has resulted in a small footprint size. For example, Hendrickx's former PhD student *Hong* [2008] conducted a comprehensive study of footprints for 12 riparian EC sites in NM, CA, and AZ for meteorological conditions at the landsat overpass time (late morning) using

the model by *Hsieh et al.* [2000]. He found that at most EC sites, the maximum contribution to the footprint is within 50 m from the tower and 80% of the integrated footprint density function are located within 100 m from the tower. Obviously these scales are much smaller than the scales required for validation and calibration of remote sensing algorithms.

Whereas typical EC footprints are on the order of 100s m^2 and cover completely different areas when the wind direction changes more than 90 degrees, the footprint areas of scintillometers are typically on the order of 10,000s m^2 and cover –at least partly– the same area when the wind direction changes more than 90 degrees. Figure 5 shows an example of a footprint weighting function for our transects in NM for late morning conditions. For SE winds (parallel to the transect) the footprint is underneath the transect, and displaced upwind of the center; 80% of the footprint weighting function is represented by an area of 1.2 km^2. Since the LAS measurements represent a line-averaged measurement, which is weighted toward the center of the transect, the footprint will typically take the shape of an ellipsoid whose extent is typically ~30% less than the actual transect length.

2.3 Scintillometer Network in New Mexico

The scintillometer network in New Mexico was located within and around the Middle Rio Grande Basin. It consisted of seven Kipp & Zonen Large Aperture (LAS) scintillometer transects at different locations representing a range of elevations (1448 – 3206 m) and land surfaces: dry homogeneous grasslands, heterogeneous moist riparian areas, dry homogeneous shrubland, moist homogeneous grassland, homogenous basalt outcrops, and homogeneous irrigated alfalfa fields (Table 1, Figures 6-7). The two principal objectives of the network were to: (1) develop efficient operating protocols and wireless infrastructure for the operation of scintillometers over a large region; and (2) develop procedures for the use of sensible heat flux measurements by scintillometers for the calibration and validation of remote sensing algorithms. These protocols and procedures are needed before a more permanent network of high-quality energy balance ground measurements can be installed in New Mexico. Although initial measurements showed reasonable agreement between the sensible heat fluxes measured with different LASs and with eddy correlation (Figure 8), the comprehensive intercomparison revealed larger biases among scintillometers as reported below in Section 4.

A: Wind Direction Parallel to Transect. **B: Wind Direction Perpendicular to Transect.**

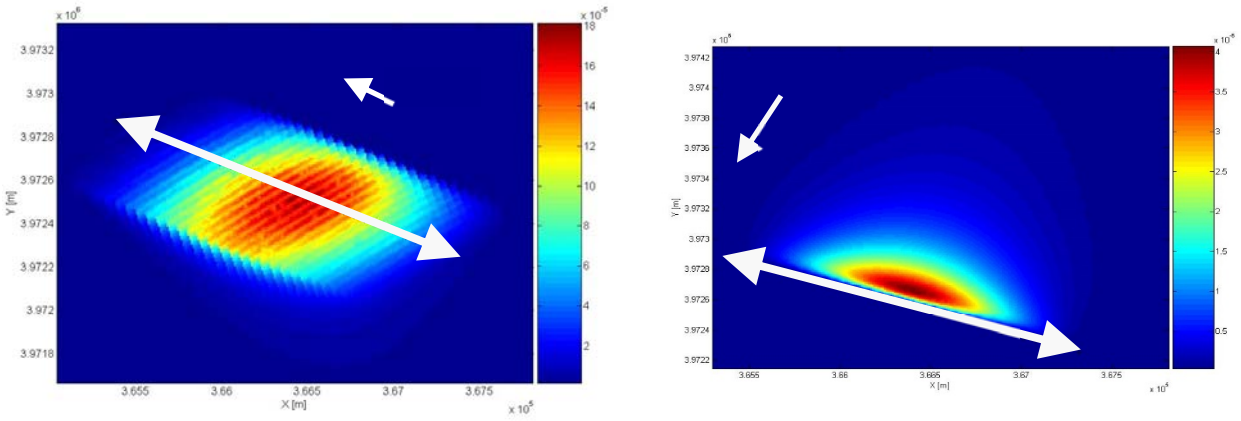

Figure 5. Typical footprint weighting function (color) for a LAS transect (white line) at the El Malpais National Monument, NM. The transect length is 2.9 km and its height above the land surface is 60 m. Note the differences in vertical scales. The footprint under perpendicular wind direction is larger than under parallel wind direction [*Meijninger et al.*, 2002].

San Acacia riparian area (SAR)

Valles Caldera mountainous grassland (VCNP)

Desert/shrubland near Socorro (EMRTC)

Low albedo lava flows (EMNM)

Figure 6. Examples of LAS setup locations in New Mexico in moist riparian areas and mountainous grasslands and dry deserts and lava flows.

Table 1. New Mexico Tech large aperture scintillometer (LAS) network [*Kleissl et al.*, 2009a]. Coordinates of the locations are given in UTM 13 WGS84 except for El Malpais NM.

SITE	**SEVILLETA NWR**	**SAN ACACIA RIPARIAN**	**EMRTC**	**VALLES CALDERA NP**	**MAGDALENA RIDGE**	**EL MALPAIS NM**	**SAN ACACIA ALFALFA**
ECOSYSTEM	DRY GRASSLAND	RIPARIAN	DRY SHRUBLAND	GRASS, MOUNTAINS	GRASS, MOUNTAINS	BASALT OUTCROPS	ALFALFA
DATA SINCE[#]	NOV 19, 2005	MAY 3, 2006	JULY 18,2006	JUNE 6, 2006	JULY 23, 2006	SEP 1, 2006	SEP 9, 2006
RECEIVER: NORTHING [M]	3795105	3791818	3770951	3972272	3761674	UTM 12 3876026	3792556
RECEIVER: EASTING [M]	345711	326400	322835	367312	298177	765019	326121
RECEIVER: ELEVATION [M]	1688	1486	1448	2675	3206	2533	1460
TRANSMITTER: NORTHING [M]	3794128	3792843	3768646	3972872	3762206	3874340	3792296
TRANSMITTER: EASTING [M]	347899	329312	320363	365401	297886	767611	324409
TRANSMITTER: ELEVATION [M]	1789	1472	1681	2678	3222	2423	1424
TRANSECT LENGTH [M]	2398	3087	3388	2003	606.3	2941	1732
EFFECTIVE HEIGHT [M]	31.5	44.8	62.9	42.6	17.6	59.8	20.0

Measurements have been suspended in 2007 to focus on the quantification of bias among scintillometers.

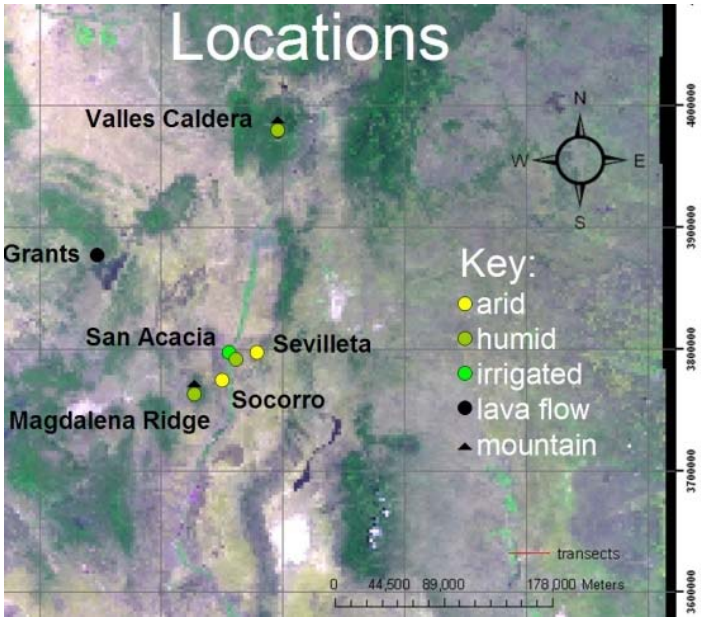

Figure 7. Locations of LAS transects in the New Mexico scintillometer network in March 2007.

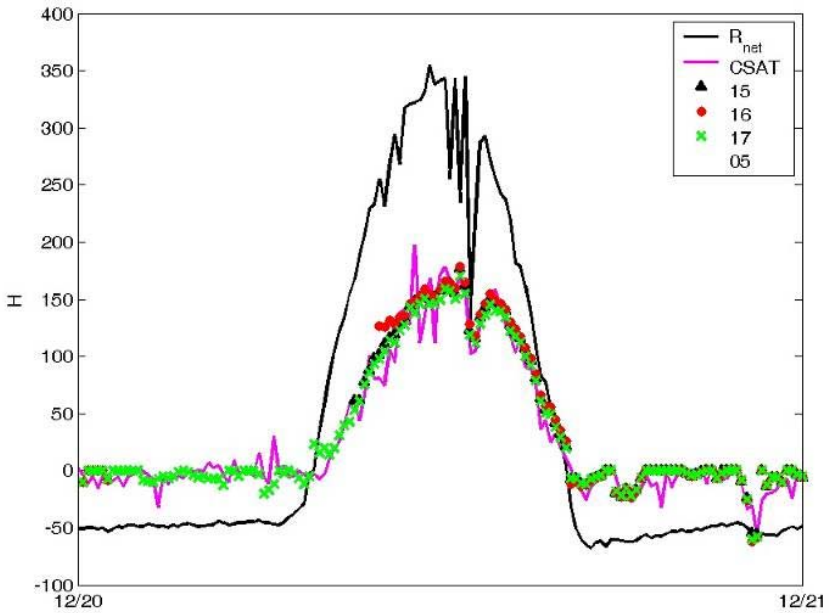

Figure 8. Intercomparison of sensible heat flux measurements from three LASs (symbols), EC (purple line), and net radiation (black line) in December 2005. The LAS measurements agree well with EC and provide a much smoother time series.

3. REMOTE SENSING ALGORITMS FOR EVAPOTRANSPIRATION

Any operational system for continuous ET mapping in the mountainous regions of the southwestern USA should be based on satellite imagery that is available on a regular basis at low cost, proven operational remote sensing ET algorithms, and relatively simple sensors to provide the energy balance and meteorological ground measurements that are needed to calibrate and validate the ET algorithms. Therefore, the authors use (1) Landsat and MODIS imagery that is available, respectively, every 16 days and daily at no cost from NASA; (2) the operational ET algorithms Surface Energy Balance Algorithm for Land (SEBAL) [*Bastiaanssen et al.*, 2005] and Mapping EvapoTanspiration at high Resolution with Internalized Calibration (METRIC) [*Allen et al.*, 2011] that are used by national and international agencies for ET mapping worldwide; and (3) scintillometry together with standard meteorological sensors for ground measurements as described in the previous section.

3.1 Landsat and MODIS Satellite Imagery

The SEBAL/METRIC approach requires satellite imagery that contains information on the energy reflected or emitted from the land surface in the visible as well as the near–, mid–, and thermal infrared parts of the electromagnetic spectrum [*Campbell*, 2007]. Different combinations of visible, near– and mid-infrared bands can be employed but thermal (surface temperature) information is critical [*Allen et al.*, 2007a]. For operational applications this imagery needs to be available frequently over the area of interest.

For the SEBAL/METRIC approach imagery from the Landsat system, especially Landsat 5 and 7, and the Moderate Resolution Imaging Spectroradiometer (MODIS) (Fig. 9) is often used since it provides multispectral information covering the optical and thermal parts of the electromagnetic spectrum at different spatial resolutions (Table 2). The spatial resolution of Landsat pixels is 30×30 m except for the thermal band that has resolutions of 120 and 60 m for, respectively, Landsat 5 and 7. The spatial resolution of MODIS varies from 250 m for visible bands to 1000 m for the thermal bands. Thus, the spatial resolution of MODIS is much coarser than that of Landsat, but its temporal resolution is daily whereas Landsat only provides one image every 16 days.

The area of interest in the satellite image needs to have a clear sky because evapotranspiration cannot be computed for cloud covered land surfaces. Even a thin layer of clouds can considerably affect the thermal band readings and cause large errors in calculation of sensible heat fluxes. In regions where cloud covers occur frequently SEBAL/METRIC applications can use a combination of Landsat (high spatial resolution, low temporal resolution) and MODIS (low spatial resolution, high temporal resolution) imagery [*Hong et al.*, 2009; 2011] to obtain sufficient information for estimation of seasonal ET [*Allen et al.*, 2007b]

Table 2. Band spatial resolutions (m) and wavelengths (μm) of Landsat 7 and MODIS sensors.

Sensors		Band number								
		1	2	3	4	5	6	7	31	32
Landsat 5&7	Pixel size [m]	30	30	30	30	30	60/ 120[#]	30	NA*	NA*
	Band width [μm]	0.45 – 0.51	0.52 – 0.60	0.63 – 0.69	0.75 – 0.9	1.55 – 1.75	10.4 – 12.5	2.09 – 2.35	NA*	NA
MODIS	Pixel size [m]	250	250	500	500	500	500	500	1000	1000
	Band width [μm]	0.62 – 0.67	0.84 – 0.87	0.46 – 0.48	0.54 – 0.56	1.23 – 1.25	1.63 – 1.65	2.11 – 2.15	10.8 – 11.3	11.8 – 12.3

[#]Spatial resolution Landsat 5 and 7, respectively, 120 and 60 m.
*Not available

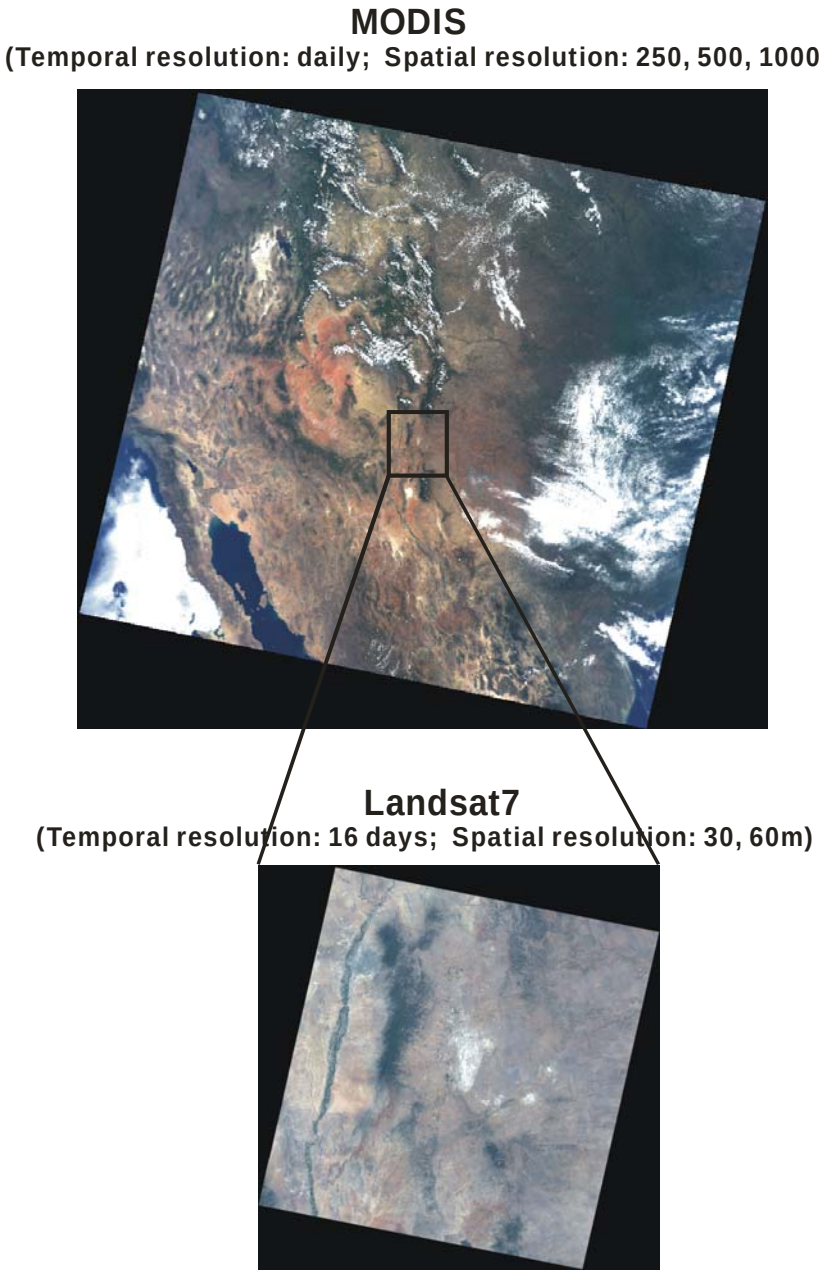

Figure 9. Landsat and MODIS satellite imagery covering the Middle Rio Grande valley on June 16, 2002.

3.2 SEBAL/METRIC Algorithms for Evapotranspiration Mapping

SEBAL [*Bastiaanssen et al.*, 1998a; *Bastiaanssen et al.*, 1998b] and METRIC [*Allen et al.*, 2007a; *Allen et al.*, 2007b] are "snapshot" energy balance models using the strong thermal signals sensed by satellites that are associated with evaporation processes to provide high resolution ET images. Spatial resolutions of retrievals range from 30 to 120 m with Landsat to 500 to 1000 m with MODIS satellite data [*Allen et al.*, 2007a; *Compaoré et al.*, 2008; *Hong et al.*, 2009]. SEBAL/METRIC energy balance algorithms are thermally driven, with ET computed as a residual of the surface energy balance, so that uncertain air humidity, air temperature, and vegetation canopy conductivities are not needed [*Allen et al.*, 2007a]. The SEBAL/METRIC approach employs an innovative Calibration using Inverse Modeling at Extreme Conditions method pioneered in SEBAL [*Bastiaanssen et al.*, 1998a; *Bastiaanssen et al.*, 1998b] to overcome biases in land surface temperature retrievals and unknown spatial variation in near surface air temperature during the estimation of sensible heat flux. The METRIC/SEBAL approach has demonstrated ET accuracies of 15, 10, and 5% for daily, monthly and seasonal timescales [*Allen et al.*, 2007b; *Bastiaanssen et al.*, 2005; *Hendrickx and Hong*, 2005; *Hong*, 2008]. SEBAL/METRIC consists of physically based image analysis algorithms and utilizes high-resolution terrain models for solar and thermal radiation calculation. SEBAL/METRIC has been successfully used with Landsat and MODIS images in numerous practical applications [*Allen et al.*, 2008b; *Bastiaanssen*, 2000; *Bastiaanssen et al.*, 2002b; *Hafeez et al.*, 2006; *Hong et al.*, 2009; 2011].

SEBAL is a remote sensing flux algorithm that solves the surface energy balance on an instantaneous time scale and for every pixel of a satellite image [*Bastiaanssen*, 2000; *Bastiaanssen et al.*, 2002a; *Bastiaanssen et al.*, 1998a; *Bastiaanssen et al.*, 1998c]. The method is based on the computation of surface albedo, surface temperature, and vegetation index from multispectral satellite data. The surface albedo is used to calculate net short wave radiation, and surface temperature for the calculation of net long wave radiation, soil heat flux and sensible heat flux. The vegetation index governs the soil heat flux by incorporating light interception by canopies, and is used to express the aerodynamic roughness of the landscape. The latent heat flux is computed as the residue of the surface energy balance. Air humidity measurements are not needed because evaporation is computed from the latent heat flux. SEBAL has been applied for

water balance estimations [*Pelgrum and Bastiaanssen*, 1996], irrigation performance assessment studies [*Roerink et al.*, 1997], and for weather prediction studies [*Van de Hurk*, 1997].

SEBAL is a physically based analytical method that evaluates the components of the energy balance and determines the ET rate as the residual

$$R_n - G - H = \lambda E \tag{6}$$

where R_n is the net incoming radiation flux density (W m^{-2}), G is the ground heat flux density (Wm^{-2}), H is the sensible heat flux density (W m^{-2}), and λE is the latent heat flux density (W m^{-2}), which basically is the ET rate. The parameter λ is the latent heat of vaporization of water (J kg^{-1}) and E is the vapor flux density (kg m^{-2} s^{-1}). Evaporation E includes both bare soil evaporation and canopy transpiration.

The main challenge in the energy balance is to determine the partitioning of the available energy ($R_n - G$) into λE and H. The net radiation R_n is estimated from the remotely sensed surface albedo, surface temperature, and solar radiation calculated using standard astronomical formulae [*Iqbal*, 1983]. The ground heat flux G is determined through semi-empirical relationships with R_n, surface albedo, surface temperature, and vegetation index [*Bastiaanssen*, 2000; *Bastiaanssen et al.*, 2002a; *Bastiaanssen et al.*, 1998a; *Bastiaanssen et al.*, 1998c]. The most critical factor in the physically based remote sensing algorithms is to solve the equation for the sensible heat (H)

$$H = \rho_a \, c_p \, \frac{T_{aero} - T_a}{r_{ah}} \tag{7}$$

where ρ_a is the density of air (kg m^{-3}), c_p is the specific heat of air (J kg^{-1} K^{-1}), r_{ah} is the aerodynamic resistance to heat transfer (s m^{-1}), T_{aero} is the surface aerodynamic temperature, and T_a is the air temperature either measured at a standard screen height or the potential temperature in the mixed layer [Brutsaert et al., 1993]. The aerodynamic resistance to heat transfer is affected by windspeed, atmospheric stability, and surface roughness [*Brutsaert*, 1982]. The apparent simplicity of Eq. [2] is deceptive since T_{aero} cannot be measured by remote sensing. Remote sensing techniques measure the radiometric surface temperature T_{rad}, which is not the same as the aerodynamic temperature. The two temperatures usually differ by 1 to 5°C. Unfortunately, an

uncertainty of 1°C in $T_{aero} - T_a$ can result in a 50 W m^{-2} uncertainty in H [*Campbell and Norman*, 1998] that could be approximately equivalent to an evaporation of 2 mm per day. Although many investigators have tried to solve this problem by adjusting r_{ah} or using an additional resistance term, no generally applicable method has been developed yet [Kustas and Norman, 1996].

SEBAL is a practical method that overcomes the problem of inferring the aerodynamic temperature from the radiometric temperature and the need for near-surface air temperature measurements by directly estimating the temperature difference between T_1 and T_2 taken at two arbitrary elevations z_1 and z_2 without explicitly solving for the absolute temperature at a given height. The temperature difference for a dry surface without evaporation is obtained from the inversion of the sensible heat transfer equation setting latent heat flux λE=0 so that H=R_n-G [*Bastiaanssen et al.*, 2002a; *Bastiaanssen et al.*, 1998a; *Bastiaanssen et al.*, 1998c]

$$T_1 - T_2 = \Delta T_a = \frac{H\, r_{ah}}{\rho_a\, c_p} \tag{8}$$

For a wet surface all available energy R_n-G is used for evaporation λE so that H=0 and ΔT_a=0. Field observations have indicated that land surfaces with a high ΔT_a are associated with high radiometric temperatures and those with a low ΔT_a with low radiometric temperatures. For example, in New Mexico and Idaho moist irrigated fields have a much lower ΔT_a than dry rangelands. Field measurements in Egypt and Niger [*Bastiaanssen et al.*, 1998c], China [Wang et al., 1998], USA [Franks and Beven, 1997], and Kenya [Farah, 2001] have shown that the relationship between T_{rad} and ΔT_a is linear

$$\Delta T_a = c_1\, T_{rad} - c_2 \tag{9}$$

where c_1 and c_2 are the linear regression coefficients valid for one particular moment (the time and date the image is taken) and landscape. *Allen et al.* [2007a] and *Allen et al.* [2011] support the linearity of Eq. [9] with theoretical arguments based on the physics of micrometeorology. By using the minimum and maximum values of ΔT_a as calculated for the coldest and warmest pixel(s), the extremes of H are used to find the regression coefficient c_1 and c_2, which will prevent outliers of H-fluxes. Thus, the semi-empirical Eq. [9] relies on spatial differences in the radiometric surface temperature rather than absolute surface temperatures, to minimize the influence of atmospheric corrections and uncertainties in surface emissivity.

Eq. [8] has two unknowns: ΔT_a and the aerodynamic resistance to heat transfer r_{ah}, which is affected by wind speed, atmospheric stability, and surface roughness. Several algorithms take a few field measurements of wind speed and treat them as spatially constant over representative parts of the landscape [*Hall et al.*, 1992; *Kalman and Jupp*, 1990; *Rosema*, 1990]. This assumption is only valid for uniform homogeneous surfaces. For heterogeneous landscapes a wind speed near the ground surface is required for each pixel. One way to overcome this problem is to consider the wind speed spatially constant at a height of 200 m above ground level. This is a reasonable assumption since at this height the wind speed is not affected by local surface heterogeneities. The wind speed at 200 m is obtained by an upward extrapolation of a wind speed measurement at 2 or 10 m assuming a logarithmic wind profile. The wind speed at each pixel is obtained by a downward extrapolation using the surface roughness, which is determined for each pixel using an empirical relationship between surface momentum roughness z_{0m} and the Normalized Difference Vegetation Index (NDVI) or the Soil Adjusted Vegetation Index (SAVI) [*Huette*, 1988]. The end result of these calculations is the determination of values for r_{ah} and ΔT_a for each pixel, which allows us to find the sensible heat flux for each pixel. After inserting R_n, G, and H into Eq. [6], the latent heat flux λE or ET rate is derived for each pixel.

Is SEBAL "old technology"? At first inspection SEBAL is quite similar to other ET estimation methods that use T_{rad} and ΔT but with one significant difference: SEBAL uses an internal calibration process that eliminates the need for actual measurements of T_{rad} and/or ΔT as well as for atmospheric corrections. SEBAL is automatically calibrated for biases through the regression calibration of Eq. [9], which is based on a cold and warm pixel. Thus, the surface temperature T_{rad} is used as a distribution parameter for partitioning the sensible and latent heat flux. ΔT_a floats above the land surface as it is indexed to T_{rad} (through calibration Eq. [9]), but it does not require actual measurements on the ground or atmospheric corrections.

SEBAL yields an estimate of the instantaneous ET (mm/hour) at the time of the LandSat overpass around 11:00 am. This hourly ET rate must then be extrapolated to obtain the daily ET. The extrapolation is done using the evaporative fraction (*i.e.,* the ratio of latent heat over the sum of latent and sensible heat), which has been shown to be approximately constant during the day. Therefore, multiplication of the evaporative fraction determined by SEBAL with the total daily available energy yields the daily evapotranspiration rate. However, in arid and semi-arid regions

the evaporative flux can increase during the day, especially over irrigated lands. Under these conditions, the method of choice is METRIC that employs the reference ET fraction over irrigated lands but uses the evaporative fraction for rainfed vegetation [*Allen et al.*, 2011]. The senior author and his research group have applied SEBAL/METRIC The senior author and his research group have applied SEBAL within the United States in New Mexico, Arizona, California, Wyoming, Illinois, and Texas as well as in Panama, Morocco, and the Volta Basin in West Africa [*Alkov*, 2008; *Compaoré et al.*, 2008; *Hendrickx and Hong*, 2005; *Hendrickx et al.*, 2005a; *Hendrickx et al.*, 2005b; *Hendrickx et al.*, 2011; *Hendrickx et al.*, 2006; *Hendrickx et al.*, 2015; *Hong et al.*, 2015].

SEBAL can be implemented with few or no ground measurements of meteorological parameters. However, when high quality hourly measurements are available of air temperature and humidity, wind speed, and incoming solar radiation, METRIC is the preferred method. Like SEBAL, METRIC computes the latent heat flux as the residual of the surface energy balance $R_n - G - H = \lambda E$. METRIC deviates from SEBAL in its use of an internal calibration of the energy balance that incorporates effects of regional advection of energy and dry air that can substantially increase ET from irrigated agriculture and riparian vegetation [*Allen et al.*, 2007a] in semiarid and arid climates. METRIC retrievals of ET, when derived from Landsat or MODIS imagery, represent snapshots of ET during late morning. These time-snapshots are extended to the day using reference ET fraction, ETrF, a concept pioneered in METRIC. The ETrF has been shown to be nearly constant over the course of a day for non-stressed vegetation [*Allen et al.*, 2007a; *Allen et al.*, 2007b], as opposed to the evaporative fraction EF, which generally increases over a day under advective conditions. The ETrF is converted to the EF after extension of data to a full day for non-stressed vegetation, and is combined with the EF method that better estimates late morning to full day relations for stressed vegetation.

4. SCINTILLOMETER INTERCOMPARISON EXPERIMENT

The New Mexico scintillometer network was the first of its kind since commercial manufacturing of LASs had just started in 2006. Initial measurements in New Mexico yielded promising results but also indicated a possible bias among different LAS instruments. Because no instrument intercomparison studies for LAS had been carried out for this novel technology, there was a clear need for establishing the accuracy of LASs before using its sensible heat flux

measurements for data assimilation of surface fluxes into mesoscale meteorological models or the validation of remote sensing evapotranspiration algorithms such as SEBAL and METRIC. In our intercomparison experiments, we did not attempt to examine the absolute accuracy of LAS sensible heat flux measurements; neither did we examine the validity of Monin-Obukov Similarity Theory nor the true sensible heat flux (as measured by a non-existing perfect sensor). However, by comparing data from up to five adjacent LAS transects over homogeneous areas with natural vegetation, we examined the robustness of the instrument and the scintillation technique. The experiment focused on ideal setups with nearly identical transect lengths and beam heights, but also analyzed some results from experiments with larger transect spacings and slant paths [*Kleissl et al.*, 2008]. For this section, the relevant experiment is the one over identical nearly horizontal transects at the Valles Caldera National Preserve since it provides a true comparison of different LAS instruments.

Five Kipp and Zonen LAS were set up over a flat grassy highland (the Valle Grande) in the Valles Caldera National Preserve (VCNP), about 15 km west of Los Alamos, New Mexico from June 6–June 29, 2006 (Table 3). Mean daily maximum and minimum air temperatures during the study were 23.6°C and 4.4°C, respectively, and only 1.5 mm of rain was recorded between May 19 and June 6, 2006 (set-up day). June was also relatively dry with the only rainfall occurring between June 6 and June 9 (16 mm) and between June 24 and June 28 (25.2 mm). The monsoon season started in July, after the end of the experiment. The instruments were elevated on two slopes that overlook the relatively flat grassland (Fig. 10). In each valley, slope receivers and transmitters were spatially alternated to form adjacent pairs of LAS transects. The distance between the outermost LASs on the same side of the transect (LAS 32 and 31) was 53.9 m at the northwest end, and 26.2 m at the southeast end. For experiment H2, the order of LAS transects from experiment H1 was inverted. The order from north to south of the transects in experiment H1 was ’31, ’17, ’05, ’15, ’32 and changed to ’32, ’15, ’05, ’17, ’31 for experiment H2. As a result, transect ’05 was not changed between H1 and H2, but ’31 was exchanged for ’32, and ’15 was exchanged for ’17. Within a transect, the receiver was not switched with the transmitter, that is, an instrument that was located at the northwest side during experiment H1 remained there for experiment H2. This resulted in identical transect geometries but different instruments, enabling us to control for the effects of slightly different footprint and transect geometry (especially beam height) and focus on comparing instruments.

Table 3. Experimental setup and LAS instruments used for intercomparison over nearly horizontal beams in the Valles Caldera National Park (after *Kleissl et al.* [2008]). The effective beam height is calculated for free convective conditions and the distance is measured between the receiver and the transmitter.

			LAS Serial Number				
Experiment	Duration		$^{0300}05$	$^{0500}15$	$^{0500}17$	$^{0600}31$	$^{0600}32$
H1	6/6/2006 – 8/2/2006	Beam Height (m)	43.9	43.5	44.1	43.9	43.1
		Distance (m)	2014	2019	2009	2013	2022
H2	6/6/2006 – 8/2/2006	Beam Height (m)	43.9	44.1	43.5	43.1	43.9
		Distance (m)	2014	2009	2019	2022	2013

Figure 10. Photograph of experimental site at the Valles Caldera National Preserve: northwest end of the transects of experiment H1 looking southeast. The instruments at the other end of the transect are invisible in a clearing on the opposite site of the valley [*Kleissl et al.*, 2008].

Two hundred waypoints were taken with a Global Positioning System (GPS) Wide Area Augmentation System (WAAS) to establish the transect profile and the beam height. The absolute accuracy of GPS-WAAS is about 1 m or 2% of the beam height. Special care was taken to determine accurately the relative height of the transmitters and receivers. Differential GPS (DGPS) measurements were taken and confirmed by laser level measurements resulting in accuracies of about 0.1 m or 0.2% in relative height of the five beams (Fig. 11). Errors in the transect length are 2 m or better and can be neglected [*Hartogensis et al.*, 2003]. An eddy-covariance (EC) energy balance tower was located 1.3 km south of the transect over homogeneous grassland (grass height 0.3–0.5 m) similar to the vegetation in the footprint of the

LAS, and it was instrumented with a Licor Li7500 open path CO2/H2O infrared gas analyzer (IRGA), a Campbell Scientific 3D sonic anemometer (CSAT3) at 2.93 m above ground level, a Kipp and Zonen NR-Lite net radiometer, and a tipping bucket rain gauge. The 20 Hz EC data were stored and corrected for coordinate rotation, frequency response, and Massman correction in postprocessing using 30-min averages. From the EC measurements, the roughness length of 0.014 m and zero displacement height of 0.01 m were determined following *Martano* [2000].

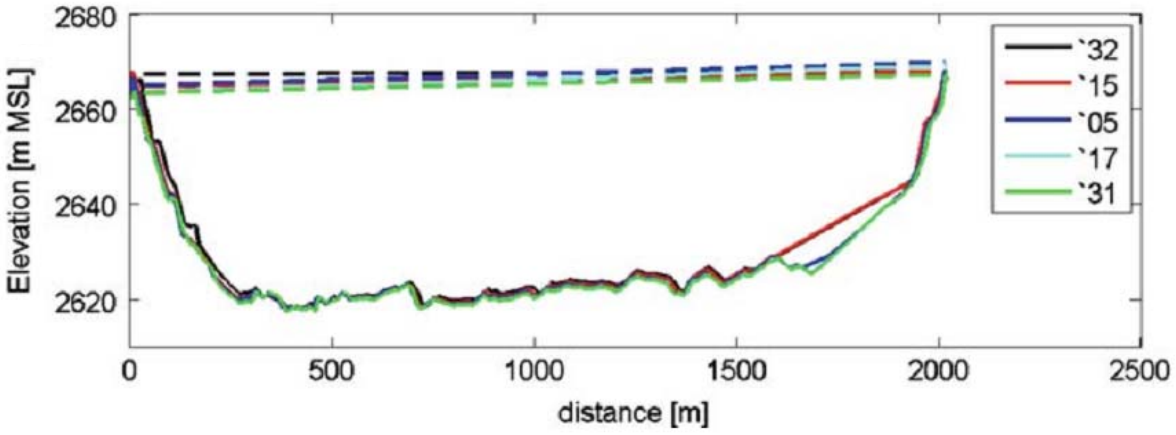

Figure 11. Profile of the transects used in experiments H1 and H2. The legend gives the last two digits of the LAS serial number (Table 3). Receivers and transmitters were alternated at each site [*Kleissl et al.*, 2008].

As suggested in the Kipp and Zonen LAS manual, data were not used when the signal strength ("demod") fell below 50 mV. Due to insufficient solar panel size and associated power outages, this happened frequently at night. For the intercomparison, only unstable daytime data are shown; unstable atmospheric conditions are almost without exception the prevailing state when clear-sky satellite imagery is captured by the Landsat and MODIS satellites. Finally, for the comparison between LAS and EC measurements, wind direction filters were applied to exclude CSAT data from a 60 degree sector in the rear of the sensor and tower.

Figure 12 presents a typical time series of the net radiation and sensible heat flux measurements from LAS and EC on June 19, 2006. Qualitatively, the LAS and EC measurements agree well in unstable (typically day time) as well as stable (typically night time) conditions. Short-term fluctuations in the sensible heat flux due to net radiation changes (e.g., at about 1445 local time in Fig. 12) can be captured with the LAS due to the short averaging time

scale of 10 min. Figure 13 shows scatter plots of sensible heat flux measurements from LAS with serial number $^{0300}05$ versus the other LASs for experiment H1. The LAS $^{0300}05$ was chosen as the reference unit since it was the only LAS not moved during the field campaign. The figure shows high correlation coefficients of greater than 0.995, which are much larger than those from intercomparisons of EC measurements (average R^2 of 0.94, *Loescher et al.* [2005]). However, the linear regression reveals significant differences between LASs. While the differences are only 6% or less between LAS '15, '32 and '05, larger differences of up to 21% were obtained for LASs '31 and '17. The regression slopes and correlation coefficients for H2 (Table 4) are similar to those from H1 and the ranking of different sensors is identical, even though their position had changed.

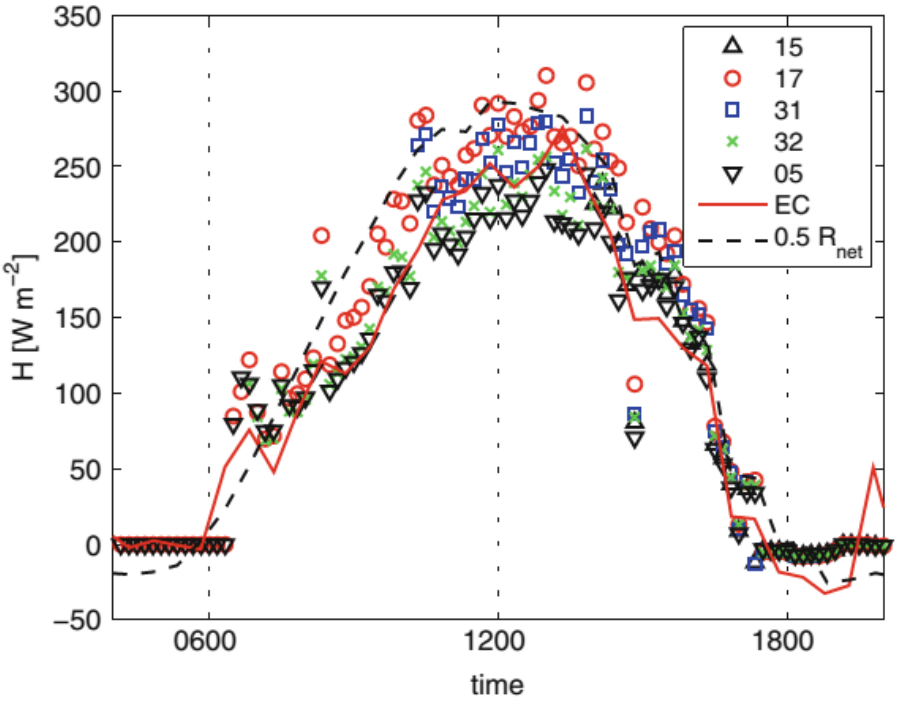

Figure 12. Example time series of the net radiation (R_{net} rescaled by 1/2) and sensible heat flux H from LAS and EC for experiment H1 on June 19, 2006 [*Kleissl et al.*, 2008].

Random errors in 10-min averages of the LAS measurements of sensible heat fluxes (H) were small since the correlation coefficients between adjacent measurements were greater than 0.995. However, linear regression of H LAS showed significant inter-instrument differences in

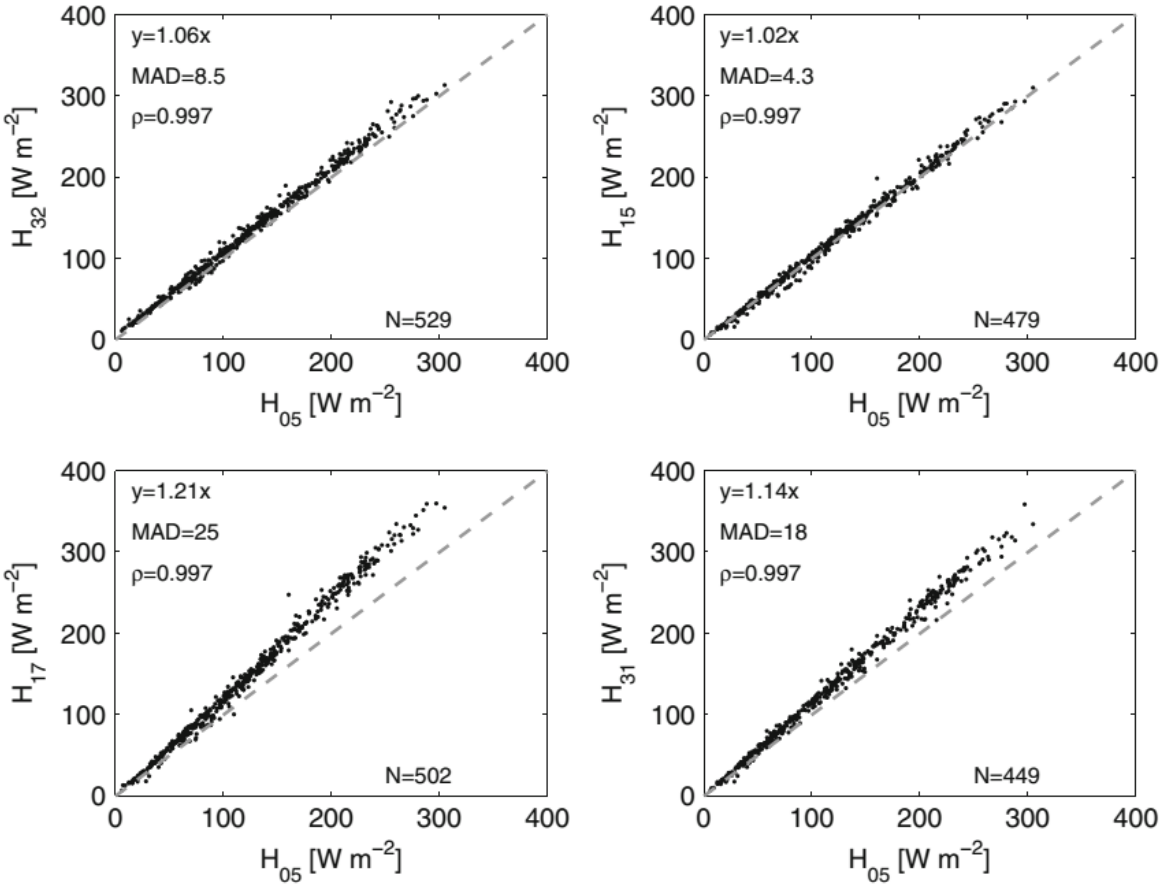

Figure 13. Scatter plots of sensible heat flux measurements from serial number $^{0300}05$ (x-axis) vs the other LASs (only the last two digits of the serial number are shown in the axis labels) for experiment H1. The text indicates the linear fit, mean absolute deviation (MAD in Wm^{-2}), correlation coefficient ρ, and number of samples N. The grey dashed line is the 1:1 line [*Kleissl et al.*, 2008].

the regression slopes that resulted in a difference in C_n^2 and H values. Experiments H1 and H2 (Table 4) allow us to examine the reasons for the differences since the setup locations were identical, with only the order of instruments changed. The regression slopes changed only slightly between H1 and H2, indicating that errors due to location, effective beam height, or external devices (e.g., dataloggers) were not responsible for the majority of the observed differences. If errors in effective beam height were responsible, then, for example, the regression slope for LAS $^{0500}15$ should have changed from 1.02 to 1.21, which was the slope for LAS $^{0500}17$ in H1 (LAS transect $^{0500}15$ and LAS $^{0500}17$ exchanged places between H1 and H2).

Table 4. Linear regression slopes and 95% confidence intervals of sensible heat fluxes between LAS-LAS and LAS-EC for the experiments H1 and H2 in unstable conditions [*Kleissl et al.*, 2008].

	LAS '32	LAS '15	LAS '05	LAS '17	LAS '31
LAS '05–H1	1.06 ± 0.01	1.02 ± 0.01	1	1.21 ± 0.01	1.14 ± 0.01
LAS '05–H2	1.11 ± 0.01	1.04 ± 0.01	1	1.16 ± 0.01	1.14 ± 0.01
EC–H1	0.91 ± 0.06	0.87 ± 0.06	0.86 ± 0.05	1.04 ± 0.06	0.96 ± 0.06
EC–H2	1.05 ± 0.12	1.01 ± 0.09	0.96 ± 0.10	1.12 ± 0.11	1.10 ± 0.10

In summary, significant inter-instrument differences in sensible heat fluxes were found. In carefully controlled experiments, this difference was as large as 21%, but typically on the order of ±6% (as measured by the median of inter-instrument differences). Errors of ±10% are typical in more realistic measurement scenarios over homogeneous natural vegetation and different transect heights and locations. To obtain errors relative to true sensible heat fluxes, errors in the auxiliary variables used to compute the sensible heat flux such as wind speed, air temperature, air pressure, roughness length, Bowen ratio and transect geometry must be taken into account, which *Hartogensis et al.* [2003] estimated to be on the order of 10%. Error propagation using our 6% consistency error estimate and the 10% error estimate of [*Hartogensis et al.*, 2003] results in a total error of 12%.

Since our LAS intercomparison experiment, several authors have confirmed our observations in other settings [*Kleissl et al.*, 2009b; *Rambikur and Chávez*, 2014; *Van Kesteren and Hartogensis*, 2011]. *Van Kesteren and Hartogensis* [2011] not only confirmed the rather large error among instruments, but they also present a thorough analysis of the causes of the errors and used an experimental setup with a lateral distance between LASs of only 1.5 m at exactly the same height. They conclude that it is possible to calibrate a LAS against a reference scintillometer in the field. Therefore, Hendrickx's MS graduate student Frank Gambardella conducted a follow-up study to investigate whether the bias of a LAS is consistent in time. He found that three of the five scintillometers used by *Kleissl et al.* [2008] maintained their bias within 3% over nearly three years. The readings of the other scintillometer differed by 12% and the last scintillometer malfunctioned due to a defective primary diode. This means that the ten scintillometers of Hendrickx research group can be used for field work in New Mexico as long as

calibration is conducted over homogeneous relatively short transects. Another option will be available soon in the form of a receiver upgrade by the manufacturer Kipp & Zonen that converts the original LAS into a second generation LAS that has been developed by the manufacturer to address the bias in the original LAS.

One major accomplishment of this project is the systematic quantification of the bias among large aperture scintillometers as published by *Kleissl et al.* [2008]. It is not the achievement that we aimed for, but it initiated the development of the next generation of LASs that will serve the hydrology community for decades to come.

Figure 14 shows the potential of scintillometry for measuring sensible heat fluxes in New Mexico over different hydrological units. The dynamics of sensible heat fluxes on 17 September 2006 depends strongly on water availability. The lowest fluxes are measured over irrigated alfalfa fields, riparian areas, and the Valles Caldera National Preserve while the highest fluxes are over low-albedo lava flows, dry grasslands, and shrublands. Due to scintillometer bias it is not possible to distinguish between the sensible heat fluxes of, for example, the low fluxes in riparian areas (SAR) and the Valles Caldera (VCNP) or the high fluxes in dry grasslands (SNWR) and shrublands (EMRTC). At the time of publication of this report, Principal Investigator Hendrickx is testing the second generation scintillometers of Kipp & Zonen that have a bias of only a few percent in the temperate humid climate of The Netherlands and United Kingdom. Figure 15 shows the first New Mexico Tech second-generation scintillometer during calibration in The Netherlands. In May 2015, this calibrated scintillometer will be tested for the semi-arid conditions of New Mexico with support of NMWRRI through a student research grant to master's graduate student Reid Brown.

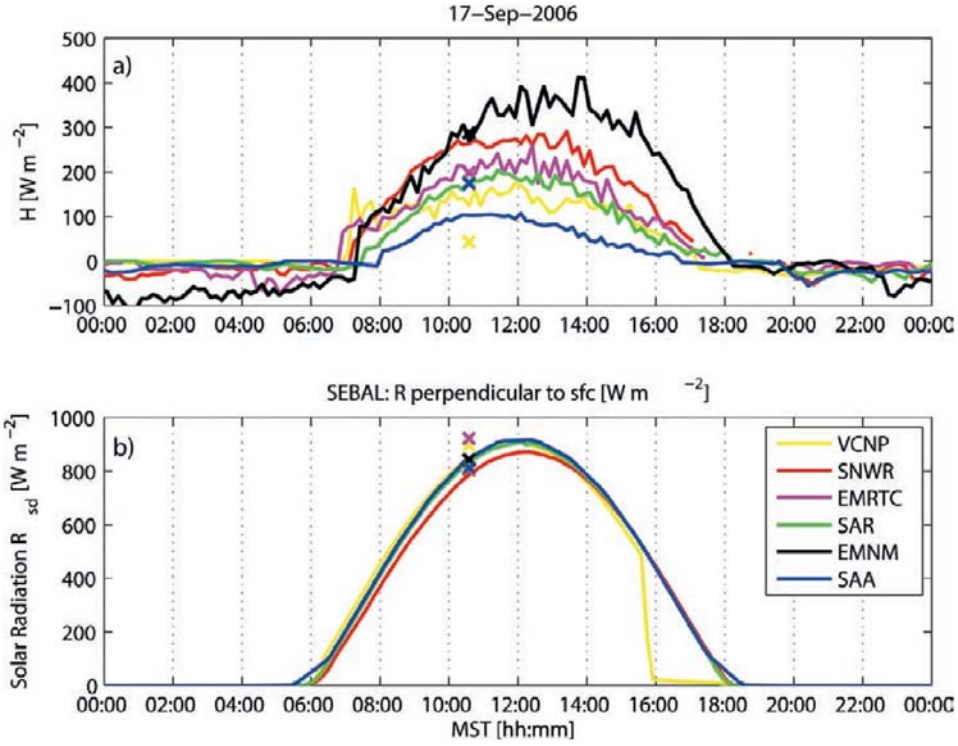

Figure 14. (top) Time series of LAS-measured sensible heat fluxes H and (bottom) global solar radiation on 17 Sep 2006. SEBAL estimates at the MODIS overpass time (1035 LST) are presented with crosses for each site. (a) On this sunny day in New Mexico, peaks of H range from less than 100 W m^{-2} over an irrigated alfalfa field (SAA) to 400 W m^{-2} over low-albedo lava flows (EMNM). Note that the EMRTC cross is right on the purple line and that the Sevilleta (SNWR, red), San Acacia riparian (SAR, green), and SAA (blue) are on top of each other. (b) The solar radiation data show a cloud-free day. SEBAL solar radiation is calculated perpendicular to the local surface, whereas the measurements show global horizontal radiation [*Kleissl et al.*, 2009a]. See Figure 7 for locations of the LAS sites in New Mexico.

Figure 15. Second generation Kipp & Zonen LAS of New Mexico Tech during calibration in The Netherlands in April 2015.

5. LESSONS LEARNED

Irrespective of the disappointing bias among individual scintillometers, the operation of the New Mexico Scintillometer Network (Table 1) has taught us many lessons on how to deploy scintillometers for the validation and improvement of remote sensing algorithms for prediction of actual evapotranspiration. These lessons will help to make the second generation New Mexico Scintillometer Network more efficient.

The length of a LAS transect strongly depends on the height of the laser beam above the soil surface and the expected maximum sensible heat flux H. The commonly reported maximum transect length of 5,000 m for a LAS is overly optimistic for natural ecosystems. For New Mexico conditions with maximum sensible heat flux over 400 Wm^{-2} a maximum transect length of 3,000 m is more realistic if the beam height can be maintained at 30 m. However, a height of 30 m does require expensive structures for mounting the scintillometer. Our experience with measurements for hydrological purposes indicates that a transect length of about 400 – 600 m is ideal: beam height will be about 2.5 – 3.0 m so that standard tripods or inexpensive pillars of cinder blocks can be used to mount the scintillometer, many areas under native vegetation in New Mexico have dimensions on a scale of a few 100s meter, a 600 m homogeneous transect fits into a 1000×1000 m MODIS thermal pixel so that comparing scintillometer ground measurements with remotely determined fluxes becomes doable. Generally, shorter transects over homogeneous areas are preferred as uncertainties in the footprint model, meteorological data, and 1-km subpixel-scale variability can accumulate to substantial errors.

From our extensive practical experience with LAS, we can attest to the fact that they are easier to operate and more robust than EC systems. Nevertheless, new LAS users can avoid pitfalls and become professional operators through training and guidance from an expert. Once a LAS is installed on a support structure that doesn't move in the wind or tilts when its soil base becomes wet and loses strength, one site visit every two months is sufficient to service the instrument. Proper functionality can be easily confirmed by observing a single variable—the receiver mean signal strength—that may weaken due to power outages or sudden or creeping misalignment between transmitter and receiver. LAS quality control can be performed easily by a dedicated undergraduate student, whereas quality control of EC systems typically requires the experience of an advanced Ph.D. student.

It is somewhat more challenging to obtain the full diurnal cycle of the sensible heat flux from an automatized data processing algorithm. Since LASs measurements do not give information about the direction of the flux, local minima in C_T^2 need to be found to determine the crossover from negative to positive and positive to negative heat fluxes around sunrise and sunset, respectively. Temperature measurements at two heights can provide information about the direction of the flux more reliably, especially over areas prone to horizontal advection of heat in the afternoon.

Last, we would like to point out some disadvantages of LAS compared to EC. Eddy covariance is based on a simple theory to measure the fluxes directly. No additional specifications of the roughness of the surface or the stability of the atmosphere are required. Eddy covariance systems provide a greater wealth of micrometeorological data than LASs, such as velocity variances and momentum fluxes in all directions.

In summary, in New Mexico we have demonstrated how LAS networks can provide valuable data and with the advent of the next generation of unbiased scintillometers, scintillometry appears a viable technology for statewide monitoring of the actual evapotranspiration.

REFERENCES

Alkov, N. (2008), Remote sensing of fire effects on Tamarisk evapotranspiration and regeneration. MS Thesis., 239 pp, New Mexico Tech, Socorro NM.

Allen, R. G. (1999), Initial report on closure error from eddy covariance systems used in the Regional Advection Perturbations in an Irrigated Desert (RAPID) – impacts on evapotranspiration *Rep.*, 12 pp, Univ. Idaho Kimberly Research and Extension Center.

Allen, R. G., and M. C. Anderson (January 2005), In telephone discussions with J.M.H. Hendrickx.

Allen, R. G., M. Tasumi, and R. Trezza (2007a), Satellite-based energy balance for mapping evapotranspiration with internalized calibration (METRIC) - Model, *Journal of Irrigation and Drainage Engineering*, *133*, 380-394.

Allen, R. G., J. M. H. Hendrickx, W. G. M. Bastiaanssen, J. Kjaersgaard, and A. Irmak (2010), Status and continuing challenges in operational remote sensing of ET, *5th National Decennial Irrigation Conference*.

Allen, R. G., M. Tasumi, A. Morse, R. Trezza, W. Kramber, and I. Lorite (2007b), Satellite-based energy balance for mapping evapotranspiration with internalized calibration (METRIC) - Applications, *Journal of Irrigation and Drainage Engineering*, *133*, 395-406.

Allen, R. G., J. M. H. Hendrickx, D. Toll, M. Anderson, W. P. Kustas, and J. Kleissl (2008a), From high overhead: ET measurement from remote sensing, *Southwest Hydrology*, *7*(1), 30-32.

Allen, R. G., A. Irmak, R. Trezza, J. M. H. Hendrickx, W. G. M. Bastiaanssen, and J. Kjaersgaard (2011), Satellite-based ET estimation in agriculture using SEBAL and METRIC, *Hydrologic Processes*, *25*, 4011–4027.

Allen, R. G., M. Tasumi, R. Trezza, C. W. Robison, M. Garcia, D. Toll, K. Arsenault, J. M. H. Hendrickx, and J. Kjaersgaard (2008b), Comparison of evapotranspiration images derived from MODIS and Landsat along the Middle Rio Grande., *ASCE-EWRI Conference* doi:10.1061/40976(40316)40987.

Anderson, M. C., J. M. Norman, G. R. Diak, W. P. Kustas, and J. R. Mecikalski (1997), A two-source time-integrated model for estimating surface fluxes using thermal infrared remote sensing, *Remote Sens. Environ.*, *60*, 195-216.

Andreas, E. L. (1989), Two-wavelength method of measuring path-averaged turbulent surface heat fluxes, *J. Atmos. Ocean. Tech.*, *6*, 280-292.

Andreas, E. L. (Ed.) (1990), *Selected papers on turbulence in a refractive medium*, 693 pp., SPIE - The International Society for Optical Engineering, Bellingham.

Bales, R. C., J. Dozier, N. P. Molotch, T. H. Painter, and R. Rice (2004), Mountain hydrology of the semi-arid western U.S. *Rep.*, 27 pp, CUAHSI Cyberseminar Draft Paper.

Bastiaanssen, W. G. M. (2000), SEBAL-based sensible and latent heat fluxes in the Irrigated Gediz Basin, Turkey, *J. Hydrol.*, *229*, 87-100.

Bastiaanssen, W. G. M., M. D. Ahmad, and Y. Chemin (2002a), Satellite surveillance of evaporative depletion across the Indus Basin, *Water Resour. Res.*, *38*, 1273-1281.

Bastiaanssen, W. G. M., M.-D. Ahmad, and Y. Chemin (2002b), Satellite surveillance of evaporative depletion across the Indus Basin, *Water Resour. Res.*, *38*(12), 1273, doi:1210.1029/2001WR000386.

Bastiaanssen, W. G. M., M. Menenti, R. A. Feddes, and A. A. M. Holtslag (1998a), A remote sensing surface energy balance algorithm for land (SEBAL): Part 1. Formulation, *J. Hydrol.*, *212-213*, 198-212.

Bastiaanssen, W. G. M., E. J. M. Noordman, H. Pelgrum, G. Davids, B. P. Thoreson, and R. G. Allen (2005), SEBAL model with remotely sensed data to improve water-resources management under actual field conditions, *J. Irrig. and Drain. Engrg., ASCE*, *131*(1), 85-93.

Bastiaanssen, W. G. M., H. Pelgrum, J. Wang, Y. Ma, J. F. Moreno, G. J. Roerink, and T. van der Wal (1998b), A remote sensing surface energy balance algorithm for land (SEBAL).: Part 2: Validation, *J. Hydrol.*, *212-213*, 213-229.

Bastiaanssen, W. G. M., H. Pelgrum, J. Wang, Y. Ma, J. F. Moreno, G. J. Roerink, R. A. Roebeling, and T. v. d. Wal (1998c), A remote sensing surface energy balance algorithm for land (SEBAL). Part 2: Validation, *J. Hydrol.*, *212-213*, 213-229.

Beyrich, F., H. A. R. De Bruin, W. M. L. Meijninger, J. W. Schipper, and H. Lohse (2002), Results from one-year continuous operation of a large aperture scintillometer over heterogeneous land surface, *Boundary-Layer Meteorology*, *105*, 85-97.

Brutsaert, W. (1982), *Evaporation into the atmosphere*, 307 pp., D. Reidel Pub. Co., Dordrecht, The Netherlands.

Brutsaert, W., A. Y. Hsu, and T. J. Schmugge (1993), Parameterization of surface heat fluxes above a forest with satellite thermal sensing and boundary layer soundings, *Jour. Appl. Meteorol.*, *32*, 909-917.

Campbell, G. S., and J. M. Norman (1998), *An introduction to environmental biophysics. Second Edition*, 286 pp., Springer, New York, NY.

Campbell, J. B. (2007), *Introduction to Remote Sensing, Fourth Edition*, 627 pp., The Guilford Press, New York, NY.

Choudhury, B. J. (1989), Estimating evaporation and carbon assimilation using infrared temperature data: Vistas in modeling, in *Therory and applications in optical remote sensing*, edited by G. Asrar, pp. 628-690, John Wiley, New York.

Compaoré, H., J. M. H. Hendrickx, S.-h. Hong, J. Friesen, N. C. van de Giesen, C. Rodgers, J. Szarzynski, and P. L. G. Vlek (2008), Evaporation mapping at two scales using optical imagery in the White Volta Basin, Upper East Ghana *Physics and Chemistry of the Earth, Parts A/B/C*, *33*, 127-140, doi:110.1016/j.pce.2007.1004.1021.

De Bruin, H. A. R. (2002), Introduction: Renaissance of scintillometry, *Boundary-Layer Meteorology 105*, 1-4.

Evett, S. R. (2000), Energy and water balances at soil-plant-atmosphere interfaces, in *Handbook of soil science*, edited by M. E. Summer, pp. A129-A182, CRC Press, Boca Raton.

Farah, H. O. (2001), Estimation of regional evaporation under different weather conditions from satellite and meteorological data. A case study in the Naivasha Basin, Kenya, 170 pp, Wageningen Univ., Wageningen.

Foken, T., F. Wimmer, M. Mauder, C. Thomas, and C. Liebethal (2006a), Some aspects of the energy balance closure problem, *Atmos. Chem. Phys.*, *6*(12), 4395-4402.

Foken, T., F. Wimmer, M. Mauder, C. Thomas, and C. Liebethal (2006b), Some aspects of the energy balance closure problem, *Atmos. Chem. Phys. Discuss.*, *6*, 3381-3402.

Franks, S. W., and K. J. Beven (1997), Estimation of evapotranspiration at the landscape scale: a fuzzy disaggregation approach, *Water Resour. Res.*, *33*, 2929-2938.

Hafeez, M., M. Andreini, J. Liebe, J. Friesen, A. Marx, and N. v. d. Giesen (2006), Hydrological parameterization through remote sensing in Volta Basin, West Africa, *Intl. J. River Basin Management*, *4*(4), 1-8.

Hall, F. G., K. F. Huemmrich, S. J. Goetz, P. J. Sellers, and J. E. Nickeson (1992), Satellite remote sensing of the surface energy balance: success, failures and unresolved issues in FIFE, *Jour. Geophys. Res.*, *97*, 19061-19090.

Hartogensis, O. K. (2006), Exploring scintillometry in the stable atmospheric surface layer, 227 pp, Wageningen University and Research Centrum, Wageningen, The Netherlands.

Hartogensis, O. K., C. J. Watts, J.-C. Rodriguez, and H. A. R. De Bruin (2003), Derivation of effective height for scintillometers: La Poza experiment in Northwest Mexico. *Journal of Hydrometeorology*, *4*, 915-928.

Hemakumara, H. M., L. Chandrapala, and A. F. Moene (2003), Evapotranspiration fluxes over mixed vegetation areas measured from a large aperture scintillometer, *Agric. Water Manage.*, *58*, 109-122.

Hendrickx, J. M. H., and S.-h. Hong (2005), Mapping sensible and latent heat fluxes in arid areas using optical imagery, *Proc. International Society for Optical Engineering, SPIE*, *5811*, 138-146.

Hendrickx, J. M. H., W. G. M. Bastiaanssen, E. J. M. Noordman, S.-h. Hong, and L. E. Calvo Gobbeti (2005a), Estimation of regional actual evapotranspiration in the Panama Canal watershed, in *The Rio Chagres: A multidisciplinary profile of a tropical watershed*, edited by R. S. Harmon, pp. 315-324, Springer, Dordrecht, The Netherlands.

Hendrickx, J. M. H., D. M. Hearer, S.-h. Hong, B. Borchers, and P. Neville (2005b), Land cover and evapotranspiration in the Middle Rio Grande Basin, *Eos Trans. AGU,* , *86(52)*, Fall Meet. Suppl., Abstract H44B-05.

Hendrickx, J. M. H., J. B. J. Harrison, B. Borchers, J. R. Kelley, S. Howington, and J. Ballard (2011), High-resolution soil moisture mapping in Afghanistan, *Proc. International Society for Optical Engineering, SPIE*, *8017*, 801710; doi:801710.801117/801712.887255.

Hendrickx, J. M. H., S.-h. Hong, J. Friesen, H. Compaore, N. C. van de Giesen, C. Rodgers, and P. L. G. Vlek (2006), Mapping energy balance fluxes and root zone soil moisture in the White Volta Basin using optical imagery, *Proc. International Society for Optical Engineering, SPIE*, *6239*, 238-249.

Hendrickx, J. M. H., J. Kleissl, J. D. Gómez-Vélez, S.-h. Hong, J. R. Fábrega-Duque, D. Vega, H. A. Moreno-Ramírez, and F. L. Ogden (2007), Scintillometer networks for calibration and validation of energy balance and soil moisture remote sensing algorithms, *Proc. International Society for Optical Engineering, SPIE*, *6565*, 65650W.

Hendrickx, J. M. H., et al. (2015), Benchmarking optical/thermal satellite imagery for estimation of evapotranspiration and soil moisture in decision support tools *Journal American Water Resources Association*, in press.

Hill, R. J. (1992), Review of optical scintillation methods of measuring the refractive index spectrum, inner scale and surface fluxes, *Wave. Random Media*, *2*, 179-201.

Hill, R. J., G. R. Ochs, and J. J. Wilson (1992a), Measuring surface-layer fluxes of heat and momentum using optical scintillation, *Boundary-Layer Meteorol.* , *58*, 391-408.

Hill, R. J., G. R. Ochs, and J. J. Wilson (1992b), Surface layer fluxes measured using the CT2-profile method, *J. Atmos. Oceanic Tech.*, *9*, 526-537.

Hong, S.-H. (2008), Mapping regional distributions of energy balance components using optical remotely sensed imagery, Ph.D. Dissertation thesis, 378 pp, New Mexico Institute of Mining and Technology, Socorro NM.

Hong, S.-h., J. M. H. Hendrickx, and B. Borchers (2009), Up-scaling of SEBAL derived evapotranspiration maps from Landsat (30 m) to MODIS (250 m) scale, *J. Hydrol.*, *370*, 122-138; doi:110.1016/j.jhydrol.2009.1003.1002.

Hong, S.-H., J. M. H. Hendrickx, and B. Borchers (2011), Down-scaling of SEBAL derived evapotranspiration maps from MODIS (250 m) to Landsat (30 m) scales, *International Journal of Remote Sensing*, *32*(21), 6457-6477.

Hong, S.-h., J. M. H. Hendrickx, J. Kleissl, R. G. Allen, W. G. M. Bastiaanssen, R. L. Scott, and A. L. Steinwand (2015), Evaluation of an extreme-condition-inverse calibration remote sensing model for mapping energy balance fluxes in arid riparian areas., *Hydrol. Earth Syst. Sci. Discuss.*, *18*, 1-61; www.hydrol-earth-syst-sci-discuss.net/18/61/2014/; doi:2010.5194/hessd-2018-2011-2014.

Horst, T. W., and J. C. Weil (1992), Footprint estimation for scalar flux measurements in the atmospheric surface layer, *Boundary-Layer Meteorology*, *59*, 279-296.

Hsieh, C.-I., G. Katul, and T.-w. Chi (2000), An approximate analytical model for footprint estimation of scalar fluxes in thermally stratified atmospheric flows, *Advances in Water Resources*, *23*, 765-772.

Huette, A. R. (1988), Soil-adjusted vegetation index (SAVI), *Remote Sens. Env.*, *25*, 89-105.
Iqbal, M. (1983), *An introduction to solar radiation*, Academic Press, Toronto.

Kalman, J. D., and D. L. B. Jupp (1990), Estimating evaporation from pasture using infrared thermography: evaluation of a one-layer resistance model, *Agr. Forest Meteorol.*, *51*, 223-246.
Khosiek, W., and M. H. A. J. Herben (1983), Evaporation derived from optical and radio wave scintillation, *Appl. Optics*, *22*, 2566-2569.

Kleissl, J., S.-h. Hong, and J. M. H. Hendrickx (2009a), New Mexico scintillometer network. Supporting remote sensing and hydrologic and meteorological models, *Bulletin American Meteorological Society*, *90*(2), 207-218, DOI:210.1175/2008BAMS2480.1171.

Kleissl, J., C. Watts, J. Rodriguez, S. Naif, and E. Vivoni (2009b), Scintillometer Intercomparison Study—Continued, *Boundary-Layer Meteorology*, *130*(3), 437-443.

Kleissl, J., J. Gomez, S.-h. Hong, J. M. H. Hendrickx, T. Rahn, and W. L. Defoor (2008), Large aperture scintillometer intercomparison study, *Boundary Layer Meteorol.*, *128*, 133–150, DOI 110.1007/s10546-10008-19274-10541.

Kumar, S. V., R. H. Reichle, C. D. Peters-Lidard, R. D. Koster, X. Zhan, W. T. Crow, J. B. Eylander, and P. R. Houser (2008), A land surface data assimilation framework using the Land Information System: description and applications, *Advances in Water Resources*, *31*, 1419-1432, doi:1410.1016/j.advwatres.2008.1401.1013.

Kustas, W. P., and J. M. Norman (1996), Use of remote sensing for evapotranspiration monitoring over land surfaces, *Hydrol. Sci. Jour.*, *41*, 495-515.

Loescher, H.W., T. Ocheltree, B. Tanner, E. Swiatek, B. Dano, J. Wong, G. Zimmerman, J. Campbell, C. Stock, L. Jacobsen, Y. Shiga, J. Kollas, J. Liburdy, and B.E. Law. (2005), Comparison of temperature and wind statistics in contrasting environments among different sonic anemometer-thermometers, *Agricultural Forest Meteorol.*, *133*, 119-139.

Martano, P. (2000), Estimation of Surface Roughness Length and Displacement Height from Single-Level Sonic Anemometer Data, *Journal of Applied Meteorology*, *39*(5), 708-715.

Marx, A. (2003), Mit SEBAL ermittelte Waermestroeme aus NOAA-AVHRR-Daten und Vergleich mit Szintillometer- und MM5-Daten in der Savannenzone Ghanas, Diplomarbeit thesis, 113 pp, Universitaet Trier.

Meijninger, W. M. L. (2003), Surface fluxes over natural landscapes using scintillometry, 176 pp, Wageningen University and Research Centrum, Wageningen, The Netherlands.

Meijninger, W. M. L., and H. A. R. de Bruin (2000), The sensible heat flux over irrigated areas in western Turkey determined with a large aperture scintillometer, *J. Hydrol.*, *229*, 42-49.

Meijninger, W. M. L., O. K. Hartogensis, W. Kohsiek, J. C. B. Hoedjes, R. M. Zuurbier, and H. A. R. de Bruin (2002), Determination of area averaged sensible heat fluxes with a large aperture scintillometer over a heterogeneous surface - Flevoland field experiment, *Boundary-Layer Meteorology 105*, 63-83.

Meybeck, M., P. Green, and C. Vörösmarty (2001), A new typology for mountains and other relief classes, *Mountain Research and Development*, *21*(1), 34-45; DOI: 10.1043/0276-4741.

Moene, A. F., W. M. L. Meijninger, O. K. Hartogensis, W. Kohsiek, and H. A. R. de Bruin (2004), A review of the relationships describing the signal of a Large Aperture Scintillometer, edited, p. 39, Dept. Meteorologie en luchtkwaliteit.

Moran, S. M., and R. D. Jackson (1991), Assessing the spatial distribution of evaporation using remotely sensed inputs, *J. Environ. Qual.* , *20*, 725-737.

Mu, Q., M. Zhao, and S. W. Running (2011), Improvements to a MODIS global terrestrial evapotranspiration algorithm, *Remote Sensing of Environment*, *115*(8), 1781-1800.

Mu, Q., F. A. Heinsch, M. Zhao, and S. W. Running (2007), Development of a global evapotranspiration algorithm based on MODIS and global meteorology data, *Remote Sensing of Environment*, *111*(4), 519-536.

Panofsky, H. A., and J. A. Dutton (1984), *Atmospheric turbulence. Models and methods for engineering applications*, 389 pp., John Wiley & Sons, New York.

Pelgrum, H., and W. B. M. Bastiaanssen (1996), An intercomparison of techniques to determine the area-averaged latent heat flux from individual in situ observations: a remote sensing approach using the European Field Experiment in a Desertification-Threatened Area data, *Water Res. Res.*, *32*, 2775-2786.

Peters Lidard, C. D., S. Kumar, Y. Tian, J. L. Eastman, and P. Houser (2004), Global urban-scale land-atmosphere modeling with the land information system, *84th AMS Annual Meeting 11-15 January 2004, Symposium on Planning, Nowcasting, and Forecasting in the Urban Zone*.

Rambikur, E. H., and J. L. Chávez (2014), Assessing Inter-Sensor Variability and Sensible Heat Flux Derivation Accuracy for a Large Aperture Scintillometer *Sensors*, *14*, 2150-2170; doi:2110.3390/s140202150.

Roerink, G. J., W. G. M. Bastiaanssen, J. Chambouleyron, and M. Menenti (1997), Relating crop water consumption to irrigation water supply by remote sensing, *Water Resources Management*, *11*, 445-465.

Rosema, A. (1990), Comparison of meteosat-based rainfall and evapotranspiration mapping of Sahel region, *Remote Sens. Env.*, *46*, 27-44.

Schmid, H. P. (1994), Source areas for scalars and scalar fluxes, *Boundary-Layer Meteorology*, *67*, 293-318.

Schmid, H. P., and T. R. Oke (1990), A model to estimation the source area contributing to turbulent exchange in the surface layer over patchy terrain, *Q.J.R. Meteorol. Soc.* , *116*, 965-988.

Schuepp, P. H., M. Y. Leclerc, J. I. MacPherson, and R. L. Desjardins (1990), Footprint prediction of scalar fluxes from analytical solutions of the diffusion equation, *Boundary Layer Meteorol.*, *50*, 355-373.

Schüttemeyer, D., A. F. Moene, A. A. M. Holtslag, H. A. R. de. Bruin, and N. v. de. Giesen (2006), Surface fluxes and characteristics of drying semi-arid terrain in West Africa, *Boundary-Layer Meteorology*, *118*, 583-612 DOI 510.1007/s10546-10005-19028-10542.

Tasumi, M., R. Trezza, R. G. Allen, and J. L. Wright (2003), US validation tests on the SEBAL model for evapotranspiration via satellite, paper presented at ICID International Workshop on Remote Sensing, Montpellier, France, Sept. 2003.

Thiermann, V., and H. Grassl (1992), The measurement of turbulent surface layer fluxes by use of brchromatic scintillation, *Boundary-Layer Meteorol.*, *58*, 367-389.

Twine, T. E., W. P. Kustas, J. M. Norman, D. R. Cook, P. R. Houser, T. P. Meyers, J. H. Prueger, P. J. Starks, and M. L. Wesely (2000), Correcting eddy-covariance flux underestimates over a grassland, *Agr. Forest Meteorol.*, *103*(3), 279-300.

Van de Hurk, B. J. J. M., W.G.M. Bastiaanssen, H. Pelgrum, and E. van Meijgaard (1997), A new methodology for assimilation of initial soil moisture fields in weather prediction models using Meteosat and NOAA data, *Journal of Applied Meteorology*, *36*, 1271-1283.

Van Kesteren, B., and O. Hartogensis (2011), Analysis of the Systematic Errors Found in the Kipp & Zonen Large-Aperture Scintillometer, *Boundary-Layer Meteorology*, *138*(3), 493-509.

Wang, J., W. G. M. Bastiaanssen, Y. Ma, and H. Pelgrum (1998), Aggregation of land surface parameters in the oasis-desert systems of Northwest China, *Hydrol. Process.*, *12*, 2133-2147.

Wang, T. I., G. R. Ochs, and S. F. Clifford (1978), A saturation resistant optical scintillometer to measure C2n, *J. Opt. Soc. Amer.*, *69*, 334-338.

Wesely, M. L. (1976a), The combined effect of temperature and humidity on the refractive index, *J. Appl. Meteorol.*, *15*, 43-49.

Wesely, M. L. (1976b), A comparison of two optical methods for measuring line averages of thermal exchange above warm water surfaces, *J. Appl. Meteorol.*, *15*, 1177-1188.